Rational Design of Substituted Diarylureas: A Scaffold for Binding to G-Quadruplex Motifs

William C. Drewe,[†] Rupesh Nanjunda,[‡] Mekala Gunaratnam,[†] Monica Beltran,[†] Gary N. Parkinson,[†] Anthony P. Reszka,[†] W. David Wilson,[‡] and Stephen Neidle*,[†]

The Cancer Research UK Biomolecular Structure Group, The School of Pharmacy, University of London, 29-39 Brunswick Square, London WC1N 1AX, U.K., and Department of Chemistry, Georgia State University, Atlanta, Georgia 30303-3083

Received June 13, 2008

The design and synthesis of a series of urea-based nonpolycyclic aromatic ligands with alkylaminoanilino side chains as telomeric and genomic G-quadruplex DNA interacting agents are described. Their interactions with quadruplexes have been examined by means of fluorescent resonance energy transfer melting, circular dichroism, and surface plasmon resonance-based assays. These validate the design concept for such urea-based ligands and also show that they have significant selectivity over duplex DNA, as well as for particular G-quadruplexes. The ligand−quadruplex complexes were investigated by computational molecular modeling, providing further information on structure−activity relationships. Preliminary biological studies using short-term cell growth inhibition assays show that some of the ligands have cancer cell selectivity, although they appear to have low potency for intracellular telomeric G-quadruplex structures, suggesting that their cellular targets may be other, possibly oncogene-related quadruplexes.

Introduction

Nucleic acids containing repetitive guanine-rich tracts can form higher-order structures, G-quadruplexes, which are held together by the G-quartet motif of four in-plane hydrogen-bonded guanines.[1−4] Quadruplex arrangements were first described for eukaryotic telomeric DNA sequences, which comprise long tandem G-tracts of simple repeats such as TTAGGG in mammals.[5,6] The terminal 3′ ends of human and other mammalian telomeres are single-stranded,[7,8] and although these are normally associated with single-stranded binding proteins such as hPOT1 in human telomeres,[9−12] they can have enhanced potential to fold up into quadruplex arrangements compared to such sequences within duplex DNA. Telomeres in normal human cells progressively shorten with successive rounds of replication[13] but are maintained in length in many cancer cells by the reverse transcriptase action of the telomerase enzyme complex.[14−18] Telomerase activity requires a linear 3′ end telomeric DNA template for transcribing, which is inhibited by folding it into a quadruplex, which can be induced by a wide range of quadruplex-stabilizing ligands.[19−36]

The potential to form quadruplexes has been established in the human and a number of other genomes and appears to have an elevated frequency of occurrence in eukaryotic promoter regions[37] notably in a number of oncogenes such as *c-myc*,[38−41] *c-kit*,[42−44] *bcl-2*,[45] and *K-ras*.[46] A quadruplex sequence has also been identified in the 5′-untranslated region of the *N-ras* oncogene.[47] The recent discovery of a functional interaction between the human nuclear protein poly ADP-ribose polymerase-1 and several quadruplexes suggests a further role for these structures.[48]

Telomere regulation and stability are achieved through a complex capping mechanism,[49−51] required to protect the chromosome ends from being recognized as damaged DNA, and are necessary for cellular viability.[52] Disruption of the capping status of the telomere results in the up-regulation of the DNA damage response system, telomere end−end fusions, and other genomic rearrangements.[51−55] It has been demonstrated that several established telomerase inhibitors,[26,56]including the trisubstituted acridine compound BRACO-19 (3,6-bis(3-pyrrolidin-1-ylpropionamido)-9-(4-dimethylaminophenylamino) acridine),[32] are able to induce rapid cellular responses of senescence and apoptosis in the absence of the characteristic lag period associated with classical telomerase inhibition.[57−60] This more rapid response has been associated with intracellular displacement of the telomeric proteins, a γH2AX/p53/p21 mediated DNA damage response and mitotic abnormalities such as telomere end−end fusions and anaphase bridges.[22,27,61−67] These observations are indicative that these ligands can have a dual action in cells, disrupting the protective capping function of the telomere, as well as acting as classic telomerase inhibitors as seen by progressive telomere shortening.

Knowledge of the details of telomeric[68−72] and genomic[38,39,43] G-quadruplex molecular structures, as well as those of G-quadruplex−ligand complexes[39,73−75] such as that involving BRACO-19,[76] can facilitate the rational design not only of new ligand analogues but also of novel G-quadruplex DNA binding scaffolds. Crystallographic studies on several telomeric quadruplex−ligand complexes have shown (1) that in all structures solved to date the quadruplexes have the all-parallel strand topology, as initially observed in the native structures and (2) the details of loop and groove geometry are variable, dependent on the nature of the individual ligand.[75,76] We have used the general features of the parallel quadruplex to rationally design a new category of nonpolycyclic quadruplex ligand that incorporates features of the inherently planar 1,3-diphenyl urea functionality, a "privileged" scaffold that has well-established druglike characteristics as well as optimal dimensions in its more stable trans−trans conformation[77,78] for efficient G-tetrad overlap (Figure 1a). This scaffold is present in a number of clinically approved and experimental therapeutic agents. We report here the design, synthesis, and evaluation of a library of molecules based around this diarylurea functionality.[78] Structure-based

* To whom correspondence should be addressed. Phone: 44 207 753 5969. Fax: 44 207 753 5970. E-mail: stephen.neidle@pharmacy.ac.uk.
[†] University of London.
[‡] Georgia State University.

10.1021/jm801245v CCC: $40.75
Published on Web 12/03/2008

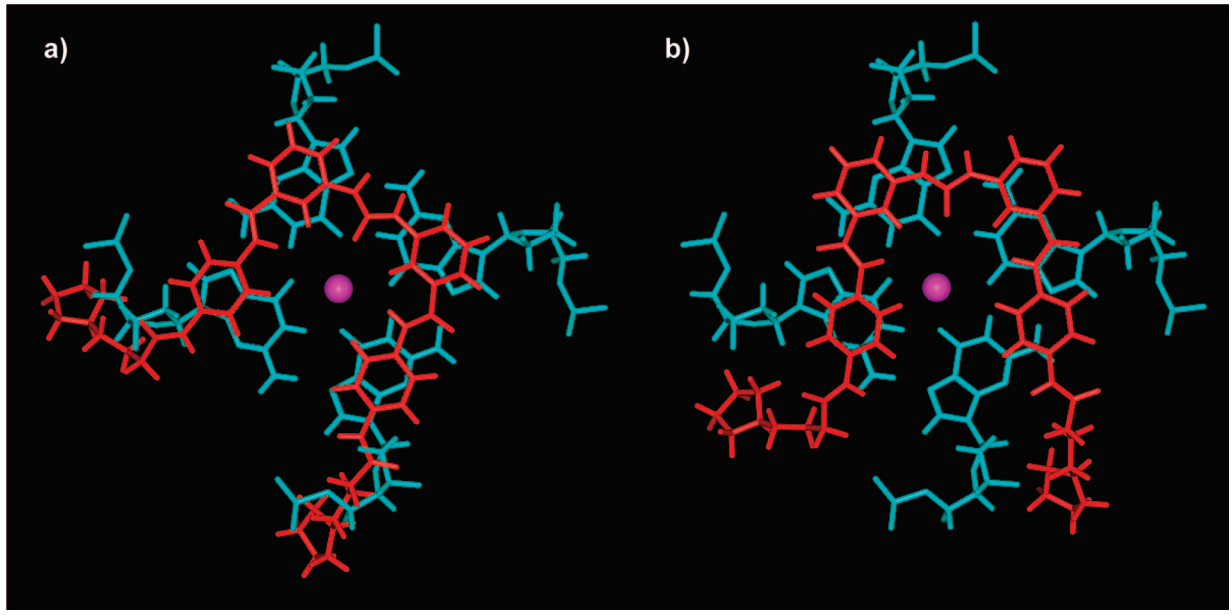

Figure 1. Molecular models showing the overlap of the diarylurea ligand **9c** (red) with a terminal G-quartet from the human parallel intermolecular quadruplex (cyan): (a) the initial idealized position with maximum overlap between phenyl rings and guanine bases, as used in the initial design concept for the series; (b) the position of the same ligand after docking and energy minimization. Note the change in orientation of the ligand, necessary in order to avoid steric clashes between the cationic substituents and quadruplex backbone atoms.

design has indicated that incorporation of additional phenylcarbamoyl groups allows all four guanine bases of a G-tetrad to be targeted, with addition of cationic side chains to enhance G-quadruplex potency and selectivity and to aid aqueous solubility.[79] These groups were systematically altered throughout the ligand series to gain an insight into structure−activity relationships (Schemes 1 and 2). Telomeric and a small set of promoter (*c-kit* and *c-myc*) G-quadruplex interactions were assessed by biophysical assays. Our ultimate aim is to develop a novel series of ligands with low levels of short-term toxicity so that cellular and ultimately in vivo administration can be undertaken at concentrations that affect telomere maintenance in cancer cells, in the absence of generalized toxic effects.

Results

Chemistry. The synthesis of compounds **9a**−**i** and **10a**−**f** was achieved through two key building blocks: the alkylaminoanilino side chains **3a**−**i** and the urea-bearing dibenzoic acids **7j**−**l** (Scheme 1).

The alkylaminoanilino side chains **3a**−**i** were synthesized from 3- and 4-nitroaniline in overall yields (three steps) of 19−99%, following methodology adapted from previously reported procedures.[30,31] Acylation was achieved by reaction with the required neat acid chloride, or the acid chloride in the presence of TEA/THF to afford **1a**−**f** in yields of 62−100%. Amination of **1a**,**b/d**,**e/g**−**i** was achieved by reaction with the required tertiary amine base (pyrrolidine/dimethylamine/piperidine/morpholine) in the presence of methanol or THF to yield **2a**,**b/d**,**e/g**−**i** in 86−100%. **1c/f** was reacted with neat pyrrolidine to yield **2c/f** in 60−88%. Catalytic hydrogenation afforded the alkylaminoanilino side chains **3a**−**i** in yields of 40−100%.

The synthesis of the diarylurea building blocks **7j**−**l** was achieved from 2-, 3-, and 4-nitrobenzoic acid in overall yields (four steps) of 33−68%. Protection of the carboxylic acid was required to avoid amide bond formation upon treatment with CDI[a] in the urea forming step[80] and was achieved with *tert*-butanol in the presence of DCC and catalytic DMAP[81] to afford **4j**−**l** in yields of 72−86%. Catalytic hydrogenation gave the amines **5j**−**l** in yields of 84−100%, which were subsequently coupled into symmetrical ureas **6j**−**l** by reaction with CDI in refluxing anhydrous THF.[82−84] **6k** was isolated following reaction with 0.6 equiv of CDI in a yield of 93% following workup, whereas **6j/l** required an additional 0.6 equiv of CDI to consume all of the starting amine. This gave **6j/l** as crude material that was used without further purification. **7j**−**l** were isolated by suspension of **6j**−**l** in TFA.[85] Isolation of the precipitate afforded **7k/l** in yields of 95−100%, whereas **7j** demonstrated enhanced TFA solubility and was isolated in 46% yield following ether precipitation.

The target ligands **9a**−**i** and **10a**−**f** were synthesized by reaction of the alkylaminoanilino side chains **3a**−**i** with the diarylurea building blocks **7k/l**. Several reagents were evaluated in order to achieve this transformation, with PyBOP in DMF[86] proving the most efficient without requiring the addition of tertiary amine base because of the basic nature of **3a**−**i**. Basic workup gave the free base of **9a**−**i** and **10a**−**f** in yields of 46−99%. The analogous reaction of the ortho-substituted **7j** with the alkylaminoanilino side chains **3a**−**f** led to cyclization of the reactive intermediate, yielding the nonplanar quinazoline dione ligands **8a**−**f** (Supporting Information).

The target ligands **15a**−**c** were synthesized from 3-amino-5-nitrobenzoic acid in overall yields (five steps) of 18−32% (Scheme 2). Amide bond formation was achieved using DCC/HOBt in DMF[87] with an excess of aniline to afford **11** in a yield of 91%. Subsequent acylation to **12a**−**c** in yields of 66−92% and amination reactions to **13a**−**c** in yields of 77−91% were achieved following the methodology discussed for the

[a] Abbreviations: FRET, fluorescent resonance energy transfer; CD, circular dichroism; SPR, surface plasmon resonance; DCC, *N*,*N*′-dicyclohexylcarbodiimide; DMAP, 4-dimethylaminopyridine; CDI, 1,1′-carbonyldiimidazole; TFA, trifluoroacetic acid; PyBOP, benzotriazol-1-yloxytripyrrolidinophosphonium hexafluorophosphate; TRAP, telomerase repeat amplification protocol; SRB, sulforhodamine B.

Scheme 1. Synthetic Route to Target Ligands **8a**−**f**, **9a**−**i**, and **10a**−**f**[a]

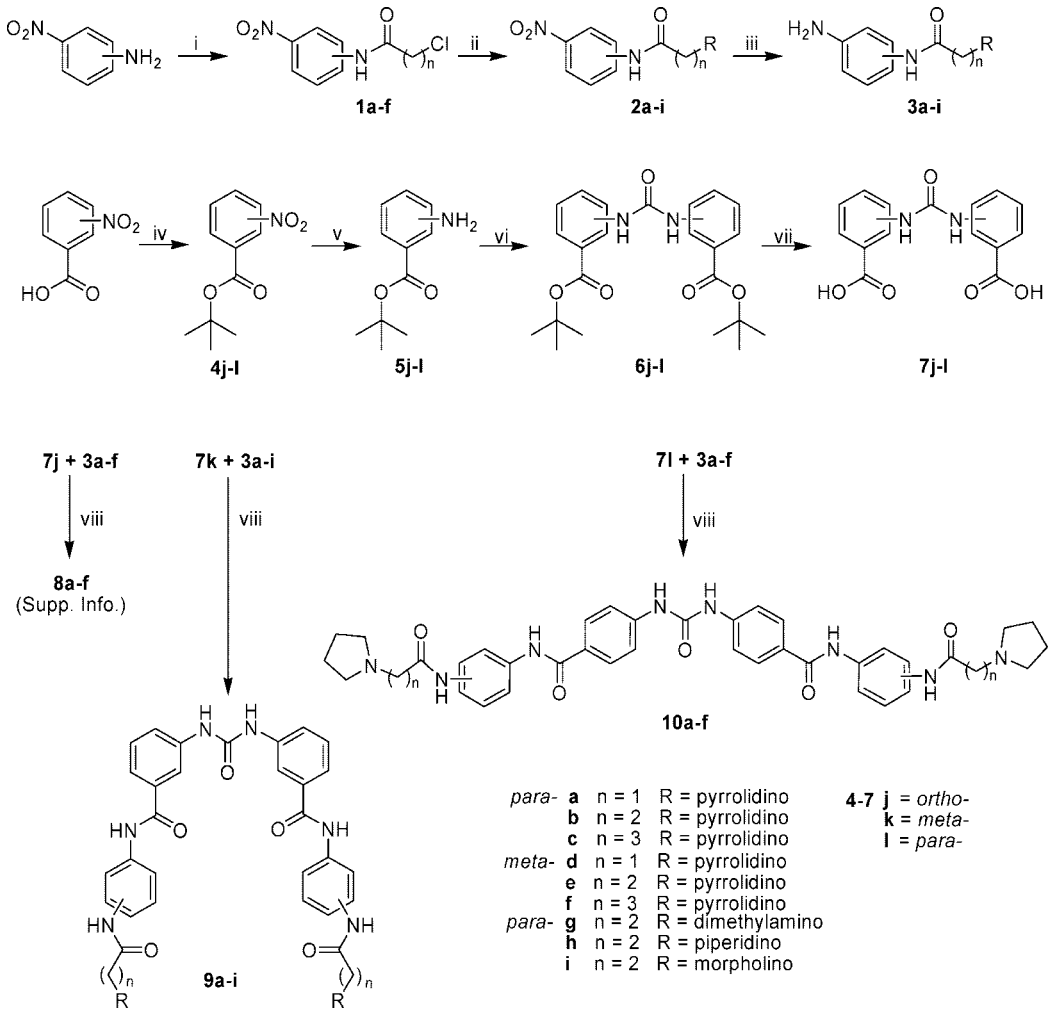

[a] (i) $Cl(CH_2)_{n=1-3}COCl$, (TEA, THF), room temp; (ii) pyrrolidine/dimethylamine/piperidine/morpholine, MeOH/THF, room temp; (iii) ammonium formate, 10% Pd/C, MeOH, room temp; (iv) ^{t}BuOH, DCC, DMAP, DCM/DMF, 0° to room temp; (v) H_2, 10% Pd/C, MeOH, room temp; (vi) CDI, THF, N_2, microwave; (vii) TFA, room temp; (viii) PyBOP, DMF, room temp.

synthesis of **2a**−**i**. In the case of the $n = 2$ side chain, elimination of HCl occurred affording the acrylamide **12b**. Catalytic hydrogenation was aided by microwave irradiation on a short time-scale to give **14a**−**c** in yields of 82−92%. Symmetrical urea bond formation was also accomplished by short time-scale microwave irradiation, with 1.0 equiv of CDI to give the target ligands **15a**−**c** in unoptimized yields of 44−56%.

The free base reaction products **8a**−**f**, **9a**−**i**, **10a**−**f**, and **15a**−**c** were purified by semipreparative HPLC to give the target ligands in suitable analytical purity for biological evaluation.

Circular Dichroism Studies. The CD spectrum of the native intramolecular human telomeric quadruplex sequence d(TTAGGGTTAGGGTTAGGGTTAGGG), corresponding to four telomeric repeats, shows a small peak at ~250 and more pronounced peaks at 270 and 288 nm (Figure 2). This spectrum is likely to correspond to a mixture of parallel and antiparallel forms, possibly including hybrid forms as well.[68−71,110−112] Five diarylureas were evaluated for their effects on this sequence, compounds **9b**, **9d**, **15b** and two further diarylureas incorporating triazole groups.[113] Figure 2 shows that the quadruplex topology is retained on binding all of these compounds, with only minor changes in the spectra being apparent, indicating that none of these ligands induce major changes in telomeric quadruplex topology on binding.

FRET Assays of Quadruplex Binding and Selectivity. A FRET (fluorescence resonance energy transfer)-based melting assay was used to assess the G-quadruplex stabilization[29,30,88] and selectivity[19,29,31,89] of the ligand library. This showed that all ligands were less effective at quadruplex stabilization than the BRACO-19 molecule.[22,32] However, they were significantly more selective for G-quadruplexes.

Ligands **9a**−**i** and **15a**−**c** are superior G-quadruplex DNA stabilizers (Table 1) compared to **8a**−**f** (Supporting Information) and **10d**−**f** (compounds **10a**−**c** were insoluble under the experimental conditions used). The ΔT_m values for **9a**−**f** show that compounds with an $n = 1$ side chain are less effective quadruplex stabilizers than the $n = 2/3$ analogues, which show approximately equivalent behavior. This pattern was, however, not consistent for compounds **15a**−**c** which demonstrate little dependence on length of the side chains. It is also apparent that the para side chain substitution pattern of compounds **9a**−**c** generally results in enhanced quadruplex stabilization except against the F21T (telomeric) G-quadruplex where little substitution pattern dependence was observed. The pyrrolidino basic group (**9b**) was consistently the most potent end-group, with compounds having piperidino (**9h**) and morpholino (**9i**) groups always showing reduced stabilization.

Inter-G-quadruplex selectivity was assessed by the relative $\Delta T_{m,1\mu M}$ values measured for the F21T (telomeric)[88] and the

Scheme 2. Synthetic Route to Target Ligands **15a**−**c**[a]

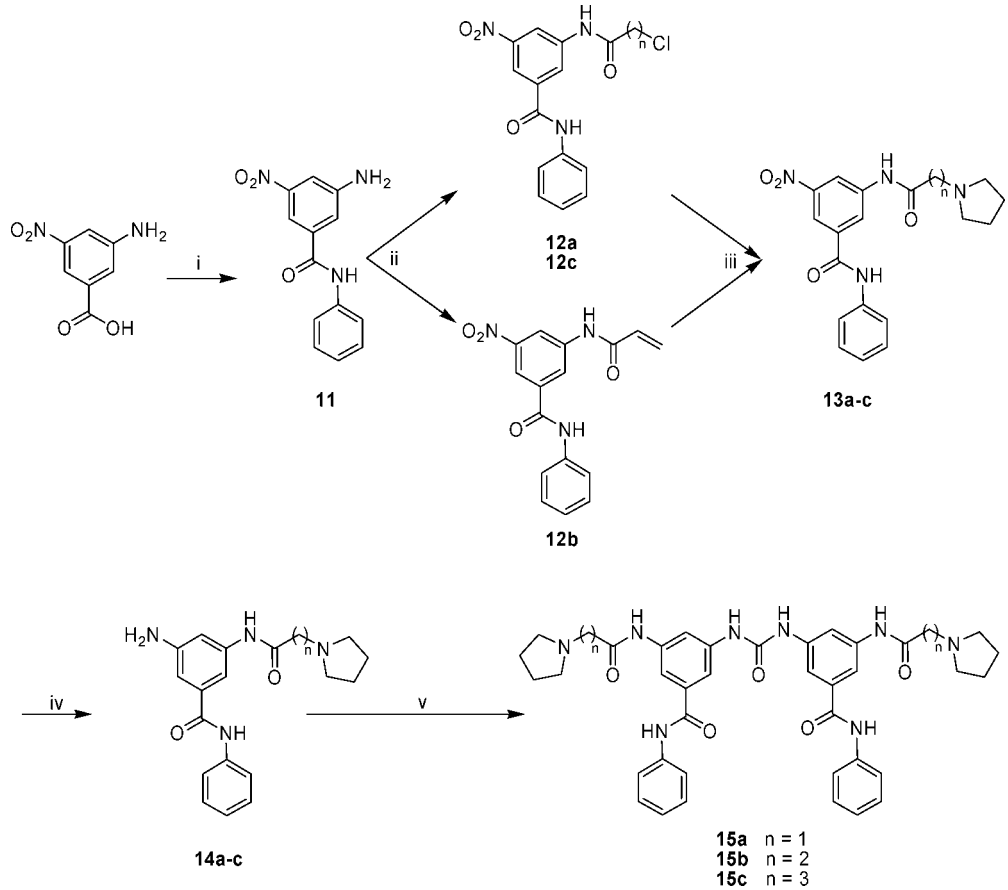

[a] (i) Aniline, DCC, HOBt, DMF, room temp; (ii) $Cl(CH_2)_{n=1-3}COCl$, TEA, THF, room temp; (iii) pyrrolidine, THF, room temp; (iv) ammonium formate, 10% Pd/C, MeOH, microwave; (v) CDI, THF, N_2, microwave.

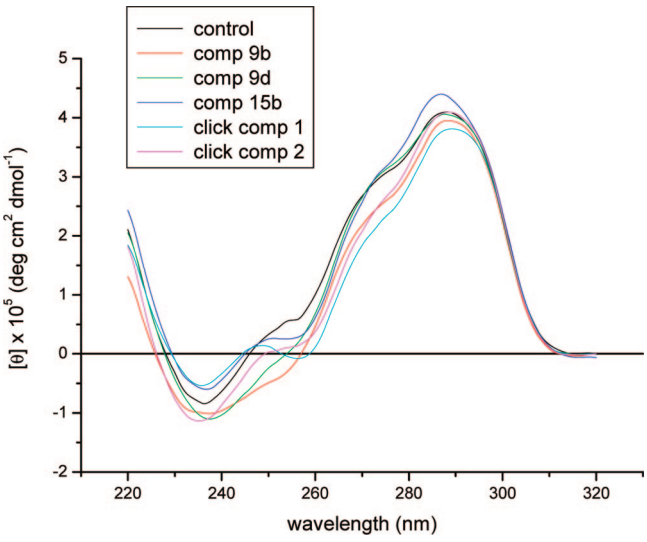

Figure 2. CD spectra of native sequence d(TTAGGGTTAGGGTTAGGGTTAGGG), marked as control, in 100 mM potassium chloride/phosphate buffer and in the presence of five different ligands **9b**, **9d**, **15b**, and two triazole-containing diarylureas.[113]

Table 1. Quadruplex and Duplex DNA FRET Assay Data Showing the Extent to Which the Ligand Stabilizes DNA Sequences against Melting[a]

	FRET ΔT_m at a 1 μM ligand concentration (°C)			
	F21T	*c-kit1*	*c-kit2*	duplex
BRACO-19	25.9 ± 0.2	20.1 ± 0.3	25.3 ± 0.4	11.2 ± 0.6
9a	7.9 ± 0.9	3.6 ± 1.1	11.3 ± 1.4	0.0 ± 0.6
9b	13.5 ± 0.6	10.2 ± 1.1	18.7 ± 1.2	0.4 ± 0.3
9c	12.0 ± 1.3	10.1 ± 0.5	17.1 ± 1.3	0.0 ± 0.6
9d	6.8 ± 0.8	3.4 ± 0.8	10.5 ± 0.6	0.3 ± 0.3
9e	14.1 ± 0.3	6.7 ± 0.7	15.3 ± 1.1	2.8 ± 0.7
9f	13.6 ± 1.3	7.8 ± 1.1	16.3 ± 0.7	0.0 ± 0.3
9g	12.3 ± 0.5	2.9 ± 1.1	13.6 ± 1.0	0.1 ± 0.2
9h	5.2 ± 0.3	7.0 ± 0.2	7.1 ± 0.6	0.1 ± 0.1
9i	1.0 ± 0.2	0.0 ± 1.1	1.3 ± 0.3	0.2 ± 0.3
10a	nd	nd	nd	nd
10b	nd	nd	nd	nd
10c	nd	nd	nd	nd
10d	1.8 ± 0.7	0.7 ± 0.5	2.0 ± 0.4	2.5 ± 0.0
10e	5.1 ± 0.9	0.5 ± 1.0	7.5 ± 0.8	4.9 ± 0.5
10f	3.3 ± 0.6	0.0 ± 0.8	6.5 ± 1.0	5.5 ± 0.6
15a	13.6 ± 0.5	5.3 ± 0.6	8.7 ± 0.3	0.0 ± 0.3
15b	13.3 ± 0.8	4.9 ± 1.2	12.9 ± 0.9	0.0 ± 0.3
15c	12.3 ± 0.6	6.3 ± 0.8	11.7 ± 0.9	0.5 ± 0.0

[a] $\Delta T_{m,1\mu M}$ is the change in melting temperature (°C) at 1 μM ligand concentration. nd represents values not determined because of insolubility.

c-kit1[43,44] and *c-kit2*[42] G-quadruplexes (Table 1). These show a broad correlation for G-quadruplex stabilization, with the selectivity trend being *c-kit2* > F21T > *c-kit1* (see Supporting Information). It is noted that the *c-kit1* G-quadruplex did not produce a simple sigmoidal melting curve in the presence of ligand (i.e., there were multiple phases to the G-quadruplex melting). Hence, the experimental melting curves were fitted to idealized sigmoid curves to enable ΔT_m values to be obtained by extrapolation (see Supporting Information).

G-Quadruplex vs duplex DNA selectivity was assessed by several FRET-based methods. Low $\Delta T_{m,1\mu M}$ stabilization of a FRET-tagged duplex DNA sequence[19,31] indicated high G-quadruplex selectivity (Table 1). Ligands **10d**−**f**, however,

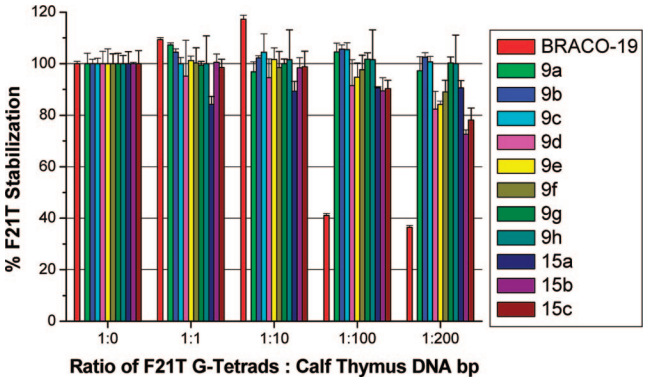

Figure 3. FRET-based competition assay data, showing the percentage of retained F21T $\Delta T_{m,1\mu M}$ stabilization when an increased ratio of calf thymus duplex DNA competitor is added.

Table 2. Quadruplex and Duplex DNA SPR Equilibrium Binding Constants ($K_A \times 10^6$ M^{-1}) for the Strong Binding Site[a]

	SPR ligand K_A ($\times 10^6$ M^{-1}) for a single-site fit				
	hTel	*c-kit1*	*c-kit2*	*c-myc*	duplex
BRACO-19[91]	31.0	na	na	na	0.5
9a	1.4	2.1	5.1	14.0	nd
9b	1.1	1.4	5.0	2.1	nd
9c	0.4	0.4	3.1	0.9	nd

[a] na, not available. nd, cannot be determined accurately because $K_A < 1.0 \times 10^3$ M^{-1}.

demonstrated comparable G-quadruplex and duplex DNA affinity. Quadruplex selectivity was further probed for the ligands **9a**−**h** and **15a**−**c** by a FRET-based competition assay[19,29,31,89] using calf thymus DNA, which demonstrated that all ligands had enhanced G-quadruplex DNA selectivity relative to BRACO-19, with the para side chain substitution pattern of compounds **9a**−**c/g/h** being optimal (Figure 3).

SPR Assays of Quadruplex Binding and Selectivity. The equilibrium binding constants of the potent and highly G-quadruplex selective ligands **9a**−**c** were assessed by surface plasmon resonance (SPR)[90,91] against quadruplex sequences originating from the human telomere (hTel), as well as from the *c-kit1/2* and *c-myc* proto-oncogenes. G-quadruplex selectivity was further assessed using a duplex DNA sequence (Table 2). Figure 4 shows example sensorgrams for ligands **9a**−**c** with *c-myc* and hTel quadruplexes, and a DNA duplex.

In terms of G-quadruplex affinity, SPR produced equilibrium binding constants that fit a single strong binding-site model with a significantly weaker secondary binding observed in most cases. In agreement with the FRET ΔT_m assay, the SPR results for hTel and *c-kit1/2* indicate that the strongest binding for each compound is to *c-kit2,* with *c-kit1* and hTel having weaker and more similar affinities (Table 2). The SPR binding constants are inversely proportional to side chain length, a trend that is not consistent with the results of the FRET assay. There is no FRET data for interactions with the *c-myc* quadruplex, but SPR results indicate inter-G-quadruplex selectivity for the *c-myc* G-quadruplex−**9a** interaction. Compound **9a** demonstrated slower dissociation kinetics, a stronger interaction and about 3-fold selectivity for the *c-myc* quadruplex (Table 2). While the affinity constants for the hTel telomeric quadruplex are reduced relative to BRACO-19,[91] the G-quadruplex/duplex DNA selectivity is significantly enhanced, with no duplex DNA interaction detected ($K_A \leq 1 \times 10^3$) under the experimental conditions used. This further confirms the G-quadruplex selectivity of ligands **9a**−**c**, which is >400- to 14000-fold (ratio $K_{Quadruplex}/K_{Duplex}$).

Molecular Modeling. Ligand structures were built using the Insight II package[92] with the CVFF force field[93] prior to assessment of the lowest energy conformations of the core structure of ligands **9a**−**i** and **15a**−**c** by manual bond rotation and minimization to convergence (root-mean-square differences (rmsd) < 0.01 kcal mol^{-1} $Å^{-1}$). Throughout this process the urea and amide bonds were maintained in their more stable trans-conformations.[77,78] This resulted in core ligand structures with all four phenyl rings coplanar. Each low-energy structure differed by 1−5 kcal mol^{-1}, suggesting that several rotamer forms may coexist (Figure 5a). The lowest-energy conformation of four in-plane phenyl rings has a square arrangement of similar dimensions to that of a G-quartet and was subsequently used for ligand building.

Following the identification of a potent single binding-site mode of G-quadruplex DNA interaction by SPR, a multistage Monte Carlo minimization simulated annealing protocol[94,95] was used to dock the synthesized ligands to the 3′ G-quartet of the parallel crystal form of the human telomeric intramolecular G-quadruplex,[68] using the CVFF force field[93] in the Docking module of Insight II.[96] This structure has been used for several previous ligand modeling studies and is supported by the consistent observation of the parallel quadruplex topology in all X-ray crystal structures of human telomeric quadruplex−ligand complexes reported to date.[75,76] A number of low-energy complex structures were predicted by this docking methodology; the urea oxygen atom was consistently predicted to be located over the ion channel of the G-quadruplex. This resulted in the optimal positioning of the diphenylurea moiety for π-stacking on the exposed G-quartet and allowed the charged side chains to penetrate the G-quadruplex grooves, forming electrostatic and hydrogen-bonding interactions. Two low-energy binding modes were predicted for these ligands: the first was demonstrated by ligands **9a**−**c**, **9h**, **9i**, and **15a**−**c** where the ligand core adopted a square conformation allowing three or four phenyl rings to simultaneously π-stack onto the G-quartet (Figures 1b and 5b). The alternative binding mode was predicted for ligands **9d**−**g** where a more extended conformation was observed so that the diphenylurea was itself optimally positioned for π-stacking and allowed the side chains to deeply penetrate the grooves (Figure 5b). It was also observed that the $n = 2/3$ side chain lengths were optimal, since the $n = 1$ side chain appeared to disrupt π-stacking of the ligand core, and that the sterically compact dimethylamino and pyrrolidino basic groups were better accommodated within the grooves relative to the more bulky piperidino group. The ligand with the uncharged morpholino end-group (**9i**) did not have electrostatic interactions with the G-quadruplex (Table 3).

The calculated interaction energies of the ligands with the G-quadruplex suggest a dependence upon the electrostatic contribution to the total energy. This also showed that all ligands have comparable overall interaction energies, with the exception of ligand **9i** with uncharged morpholino end-groups and ligands **9a** and **9d** with $n = 1$ side chains (Table 3).

The G-quadruplex vs duplex DNA selectivity of ligands **9a**−**c** was also examined using a multistage Monte Carlo minimization simulated-annealing procedure, docking the ligands to both the duplex DNA major and minor grooves, as well as to a pseudointercalation site built at the GC-step of a 10-mer B-form duplex DNA of sequence analogous to the FRET-based duplex DNA oligonucleotide.[95] It was found that the planar aromatic core of ligands **9a**−**c** was sterically too large (~10.6−13.3 Å) relative to the pseudointercalation site in the DNA duplex (~9.2 Å) to allow significant DNA intercalation. The ligands were

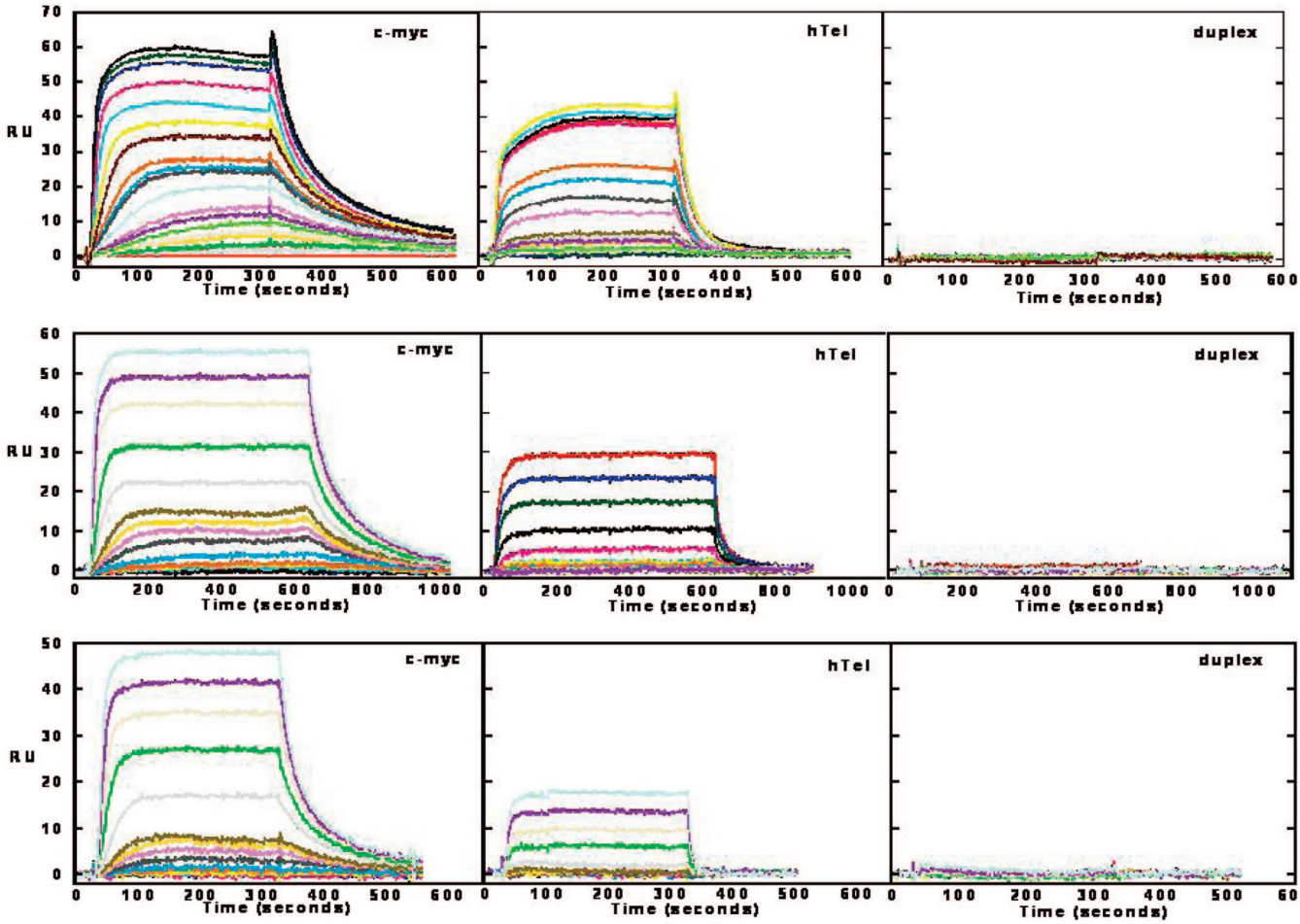

Figure 4. SPR sensorgrams for compounds **9a** (top), **9b** (middle), and **9c** (bottom) with immobilized sequences for the *c-myc* and hTel quadruplexes, and a DNA hairpin duplex (sequences are given in the Experimental Section).

well accommodated in the duplex DNA grooves; however, docking into the minor groove resulted in disruption of Watson−Crick DNA base pairs,[97] leading to duplex DNA destabilization (Supporting Information). Hence, interaction with the DNA minor groove was discounted on structural stability grounds. Assessment of the interaction energies of these docked models demonstrated that binding to the G-quadruplex was significantly favored relative to DNA duplex intercalation and major groove binding (Table 4). This is consistent with the proposed G-quadruplex/duplex DNA selectivity demonstrated by these ligands in the biophysical assays.

TRAP Assay of Telomerase Activity. The ability of ligands **9a**−**c**, **9f**, and **9g** to inhibit telomerase activity in vitro was assessed by a modified TRAP assay, the TRAP-LIG assay.[98] This enables the quantification of telomerase inhibition by removal of the ligand which can inhibit the PCR amplification step of the TRAP assay. Ligands **9a**−**c**, **9f**, and **9g** were all found to be inactive telomerase inhibitors up to the limit of solubility, with EC_{50} values of >50 μM. This indicates that neither changing the linkage from para to meta nor altering the length of the terminal side chain results in telomerase inhibition.

Cell Biology. Effects of ligands on cell growth were assessed using a panel of cancer cell lines by means of the SRB assay[99,100] to give IC_{50} values. The cancer cell lines screened include the non-small-cell lung carcinoma cell line A549 and the breast adenocarcinoma cell line MCF7. The fetal lung somatic cell line WI38 was used as a model for normal human cells to allow assessment of cancer cell selectivity.

The SRB assay results show that the MCF7 cell line was generally the most sensitive to the ligands, with **9b**, **9h**, and **10e** having low micromolar IC_{50} values, comparable to that of BRACO-19[22] (Table 5). A more limited growth inhibition response was observed with the A549 cell line, with ligands **9b** and **10e** again demonstrating behavior comparable to that of BRACO-19.[22] Selective toxicity for cancer cell lines was assessed by the ratio of the IC_{50} values for the MCF7 and A549 cell lines relative to that of the somatic control line WI38. This showed that compounds **9c**, **9h**, and **10e** are the most cancer cell selective agents; however, a potential "therapeutic window" does exist for several other ligands. Compounds **9d**−**f** and **15a**−**c** show little discrimination between cancer and normal cell lines.

Longer-term (1 week) exposure of MCF7 cells to subtoxic concentrations of ligands **9a**−**c**, **9h**, and **10e** resulted in a 0−60% reduction in cellular population doublings relative to an untreated control, which was associated with a 1−4% incidence of cellular senescence as assessed by the β-galactosidase assay[101] (Table 6). Assessment of chromosomal end−end fusions[64] was undertaken for ligand **9b** and did not show significant changes relative to an untreated control (data not shown).

Discussion

This study has validated the design concept of nonpolycyclic ligands based on the diarylurea skeleton as effective quadruplex-binding ligands coupled with a high level of selectivity over

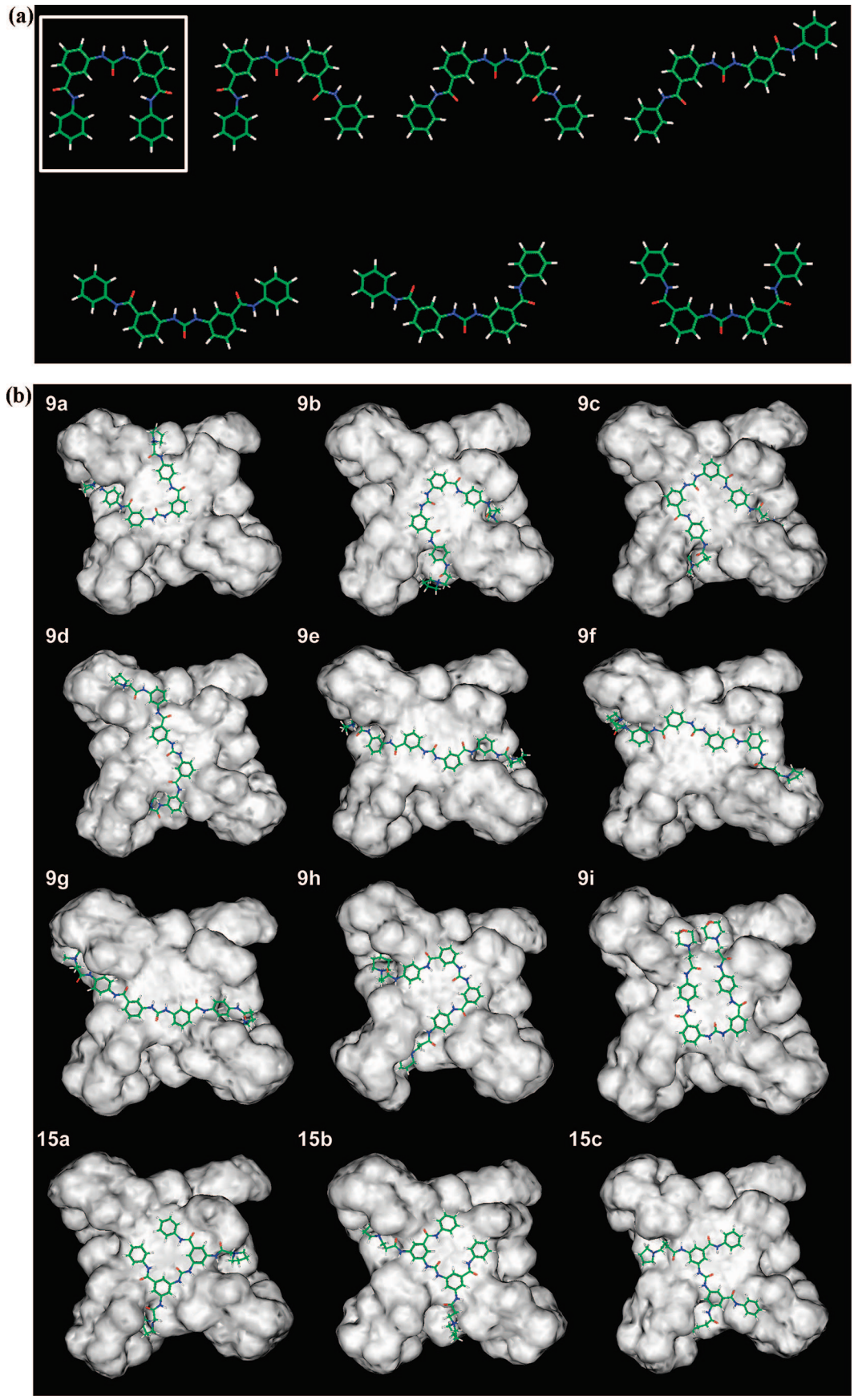

Figure 5. Molecular models of ligands and quadruplex-ligand complexes. (a) Energy minimized all-trans conformation (rmsd < 0.01 kcal mol^{-1} $Å^{-1}$) cores of ligands **9a**−**i** and **15a**−**c**. Each structure falls within a 1−5 kcal mol^{-1} energy range, and the lowest energy structure is indicate (hydrogen atoms are shown in white, carbon is shown in green, nitrogen in blue, and oxygen in red). (b) Low-energy ligand−telomeric G-quadruplex complexes found for ligands **9a**−**i** and **15a**−**c**.

Table 3. Calculated Ligand−Telomeric Quadruplex DNA Docking Interaction Energies (kcal mol^{-1})

	G-quadruplex interaction energy		
	total energy	van der Waals	electrostatic
9a	−1103.23 ± 13.61	−101.06 ± 3.21	−1002.17 ± 12.83
9b	−1157.49 ± 7.33	−102.39 ± 3.02	−1055.07 ± 7.42
9c	−1177.01 ± 16.24	−105.31 ± 3.79	−1071.66 ± 18.56
9d	−1102.44 ± 10.98	−94.20 ± 5.04	−1008.24 ± 14.99
9e	−1188.99 ± 14.71	−96.98 ± 3.10	−1092.01 ± 12.96
9f	−1171.68 ± 28.58	−103.69 ± 3.56	−1069.80 ± 27.58
9g	−1140.28 ± 34.06	−89.54 ± 4.37	−1050.74 ± 31.76
9h	−1132.65 ± 25.47	−102.92 ± 2.94	−1029.72 ± 25.30
9i	−134.71 ± 5.52	−92.02 ± 2.39	−42.68 ± 6.48
15a	−1174.23 ± 17.09	−100.89 ± 3.44	−1073.36 ± 16.11
15b	−1182.22 ± 19.06	−102.35 ± 2.98	−1079.88 ± 20.41
15c	−1167.67 ± 16.91	−103.31 ± 2.66	−1064.37 ± 16.35

Table 4. Calculated Ligand−Duplex DNA Docking Interaction Energies (kcal mol^{-1}) for Three Binding Modes

	duplex interaction energy		
	intercalation	major groove	minor groove
9a	−966.99 ± 15.02	−1011.11 ± 18.65	nr[a]
9b	−956.87 ± 10.39	−971.71 ± 28.95	nr[a]
9c	nr[b]	−1027.70 ± 10.63	nr[a]

[a] nr: no result due to duplex DNA destabilization. [b] nr: no result due to no suitably pseudointercalated structure observed.

Table 5. SRB IC_{50} Data (μM)[a]

	SRB IC_{50}			
	MCF7	A549	WI38	selectivity ratio MCF7/A549/WI38
BRACO-19[22]	2.5	2.4	10.7	4.3:4.5:1.0
9a	14.4 ± 2.8	>50.0	16.4 ± 1.3	1.1:0.3:1.0
9b	2.6 ± 0.3	5.3 ± 1.0	7.5 ± 2.9	2.9:1.4:1.0
9c	11.1 ± 0.8	>50.0	>50.0	4.5:1.0:1.0
9d	34.1 ± 2.0	>50.0	22.8 ± 2.3	0.7:0.5:1.0
9e	14.4 ± 1.5	>50.0	19.5 ± 1.9	1.4:0.4:1.0
9f	49.6 ± 6.0	>50.0	26.4 ± 5.4	0.5:0.5:1.0
9g	12.2 ± 0.6	>50.0	>50.0	4.1:1.0:1.0
9h	5.1 ± 1.4	>50.0	>50.0	9.8:1.0:1.0
9i	40.6 ± 8.4	>50.0	>50.0	1.2:1.0:1.0
10a	>25.0	>25.0	>25.0	1.0:1.0:1.0
10b	nd	nd	nd	nd
10c	nd	nd	nd	nd
10d	>50.0	>50.0	>50.0	1.0:1.0:1.0
10e	3.2 ± 1.1	4.3 ± 1.1	>50.0	15.6:11.6:1.0
10f	19.5 ± 2.0	19.4 ± 1.7	>25.0	1.3:1.3:1.0
15a	21.9 ± 2.8	>50.0	13.8 ± 1.6	0.6:0.3:1.0
15b	32.4 ± 2.2	41.5 ± 3.0	16.2 ± 1.1	0.5:0.4:1.0
15c	24.2 ± 1.9	30.6 ± 5.6	11.0 ± 1.2	0.5:0.4:1.0

[a] nd represents values not determined because of insolubility.

duplex DNA, as shown by molecular modeling and biophysical data. The exceptionally low level of duplex DNA binding is due to poor shape complementarity and consequent disruption of duplex DNA structure. Although ΔT_m and affinities are not the highest reported for quadruplex-binding ligands,[19,20] the data presented here suggest that future analogue development to improve affinity is a desirable goal, especially since diarylureas have an inherently druglike skeleton.

Chemistry. The synthesis of the target ligands **9a**−**i**, **10a**−**f**, and **15a**−**c** was achieved in reasonable (unoptimized) yields and high purity, suitable for biological analysis. The synthesis of the 2-substituted target ligands was, however, not achieved by this methodology, unexpectedly leading instead to the quinazoline dione compounds **8a**−**f** (see the Supporting Information, structure confirmed by IR spectroscopy[102−105]). Alternative synthetic strategies were considered for the synthesis of the 2-subtituted targets. However, the cyclization reaction was thought to be favored in all cases because of the proximity of the ortho-substituted phenylcarbamoylamide nitrogen of the alkylaminoanilino side chain to the imidazole-1-carboxamide intermediate in the urea forming step.

Table 6. Long-Term (1 Week) Effects on MCF7 Cell Growth[a]

	concentration (μM)	PD[b]	% of control (vc)[c]	% senescence[d]
vc		4.11 ± 0.34	100.0 ± 8.3	0.7 ± 0.2
9a	5.00	3.79 ± 0.12	92.2 ± 3.0	1.0 ± 0.3
	10.00	3.00 ± 0.38	73.1 ± 9.2	1.7 ± 1.6
9b	1.00	4.53 ± 0.07	110.4 ± 1.8	1.1 ± 1.1
	1.75	4.50 ± 0.03	109.6 ± 0.73	3.1 ± 0.2
	2.25	2.73 ± 0.20	66.5 ± 5.0	2.4 ± 0.7
9c	3.50	3.94 ± 0.24	96.0 ± 5.9	1.6 ± 0.9
	7.00	3.35 ± 0.03	81.5 ± 0.8	3.1 ± 0.4
9h	2.00	3.66 ± 0.00	89.2 ± 0.0	1.29 ± 0.0
	3.50	3.46 ± 0.34	84.3 ± 8.2	1.33 ± 0.8
11e	1.00	3.40 ± 0.26	82.9 ± 6.3	3.0 ± 0.4
	2.00	1.81 ± 0.10	44.0 ± 2.4	4.1 ± 1.2

[a] vc represents experiments performed solely with a vehicle control. [b] PD, population doublings ± sd for 1 week MCF7. [c] Percentage of 1 week population doublings normalized to the control (vc = 100%) ± sd. [d] Percentage of senescent cells assessed by the β-galactosidase assay ± sd.[101]

Biophysical Assays and Molecular Modeling of DNA Interactions. The ligands were screened by a FRET assay to give an indirect measure of G-quadruplex binding ability through assessment of thermal stabilizing potential at a specified concentration.[34,88,106] The trend in $\Delta T_{m,1\mu M}$ values for each ligand (the change in melting temperature induced by a ligand concentration of 1 μM) is in broad accord with the requirement for ligand planarity; thus, the nonplanar quinazoline dione ligands **8a**−**f** give only low ΔT_m values with all G-quadruplex DNA sequences (Supporting Information). The global conformation of the ligand core was also shown to be an important factor for efficient G-quadruplex DNA interaction, with the linear analogues **10a**−**f** having only a very weak stabilizing capability with all G-quadruplex DNA sequences (some compounds were insoluble under the experimental conditions used). These particular ligands also have comparable duplex and G-quadruplex DNA affinities, which may result from the structural similarity that these ligands have with duplex DNA groove binding ligands.[107]

The CD studies show that interactions of the human telomeric intramolecular quadruplex with a representative set of compounds result in a retention of the solution topologies, which indicates that both parallel and antiparallel forms may be present.[110−112] Molecular modeling has been performed on the parallel form, in accord with several ligand−quadruplex crystal structures[75,76,114] and the finding that the parallel form is preferred in concentrated solution akin to a cellular environment.[115] Modeling predicts that the core of ligands **9a**−**i** and **15a**−**c** can form a "square planar" conformation of similar dimensions to a G-quartet; however, several other core conformations of comparable energy were also predicted (Figure 5a). The low-energy square planar core would, however, result in optimal G-quadruplex DNA affinity due to enhanced π-stacking interactions between the four phenyl rings and the guanine bases of the G-quartet, in accord with the experimental findings in the FRET assay of enhanced G-quadruplex DNA stabilizing ability relative to ligands **8a**−**f** and **10a**−**f**. This is generally in accord with SPR binding data for ligands **9a**−**c**, which fit a single strong binding-site mode of G-quadruplex interaction. Further assessment of the potential molecular interactions was obtained by a molecular docking protocol, which found several low-energy binding conformations for these ligands; however, the square planar conformation in which the urea oxygen atom

was consistently orientated over the ion channel of the G-quadruplex was often observed. The positioning of the urea bond is possibly the result of a weak electrostatic attraction to the cationic ion channel or a secondary result of the optimal orientation of the π-stacked diphenylurea moiety. It is noted that a more extended conformation for bound ligands was also observed, which may represent the conformational diversity predicted for the ligand core. Qualitative assessment of the two predicted core substituted urea conformations indicated that the more extended core is not optimal for π-stacking interactions on the G-quartet; however, this is not reflected in the calculated interaction energies of the complexes, which is possibly the result of the force field overemphasizing electrostatic contributions to the binding. In general calculated energies in this study can only provide semiquantitative indications of properties, since implicit solvent is used in the simulations and the effects of metal ions in quadruplexes are challenging to model precisely.

The FRET assay results for ligands **9a**−**i** and **15a**−**c** show that the G-quadruplex stabilization ability of these ligands depends to some extent upon the length of the alkylamino side chains, with the side chain length of **9a** and **9d** ($n = 1$) always being inferior to those of **9b/c** or **9e/f** ($n = 2/3$), which are approximately comparable. This pattern is not, however, shown by ligands **15a**−**c**, which have reduced side chain length dependence. The results of the docking study are consistent with these results with a qualitative assessment of the generated low-energy complexes showing that the side chains are generally able to be deeply buried in the G-quadruplex DNA grooves, making several electrostatic and hydrogen-bonding contacts; however, the $n = 1$ side chain was inferior to the $n = 2/3$, since forming favorable interactions within the grooves affected the orientation of the aromatic core on the G-tetrad surface, altering the π-stacking of the ligand. This effect is shown by the order of calculated interaction energies for these complexes. The high correlation between calculated interaction energies and the FRET-based $\Delta T_{m,1\mu M\ values}$ (Supporting Information) ($r = -0.833$) indicates the predictive value of this docking method for the design of further ligands in this series.

The side chain length dependence of G-quadruplex interaction was also assessed by SPR measurements. The results did not correlate with the FRET observations, although this is probably too small a sample from which to draw firm conclusions. SPR results indicate that the $n = 1$ side chain of **9a** is optimal for general G-quadruplex DNA interaction over **9b** ($n = 2$) and **9c** ($n = 3$). It may be that in this instance affinity and thermal stability cannot be directly compared. For the hTel, *c-kit1/2*, and duplex DNAs where FRET and SPR results can be compared, there is, however, good agreement (Tables 1 and 2).

Variations in the basic end-groups were also assessed by the FRET assay. This showed that for the telomeric and *c-kit2* G-quadruplexes, the pyrrolidino (**9b**) and the dimethylamino basic groups (**9g**) resulted in superior quadruplex stabilization compared to the piperidino group (**9h**). Qualitative examination of the predicted molecular interactions of the ligand−telomeric G-quadruplex complexes indicated that this may result from the decreased steric bulk of the pyrrolidino and dimethylamino basic groups, which the modeling suggests are well accommodated in the DNA grooves relative to the piperidino group. The FRET assay results also indicate that the introduction of the nonbasic morpholino group (compound **9i**) is deleterious for all G-quadruplex sequences examined here, with docking to the telomeric quadruplex suggesting that this may result from poor groove penetration, a direct result of the absence of cationic charge at physiological pH, thus minimizing electrostatic contribution to the predicted interaction energy. The dimethylamino ligand **9g** also has a low $\Delta T_{m,1\mu M}$ value with the *c-kit1* G-quadruplex, which has no explanation in the absence of a detailed structural model for this complex.

Examination of potential selectivity between different G-quadruplexes as assessed in the FRET assay (comparison of the $\Delta T_{m,1\mu M}$ values) shows for any one compound a broad correlation with G-quadruplex DNA affinity, which may be expected since the ligands were initially designed to interact generally with G-quadruplexes (focusing on G-quartet recognition) and not for a specific G-quadruplex. However selectivity, generally in the order *c-kit2* > F21T > *c-kit1* G-quadruplexes is apparent. The *c-kit1* G-quadruplex was observed to melt in a nonsigmoidal manner (Supporting Information), which may result from the structural difference between the *c-kit1* and other G-quadruplex folds.[38,39,43,68−72] The SPR results indicate a distinct order of selectivity with *c-myc* > *c-kit2* > *c-kit1* > F21T, with the interaction of ligand **9a** being particularly enhanced for the *c-myc* quadruplex, which also has slower dissociation kinetics. It is noted that the FRET-based assessment of the interactions of these ligands with the *c-myc* G-quadruplex is not possible under the experimental conditions used because of the exceptional stability of this quadruplex fold.

The best agreement between the FRET and SPR assays is for G-quadruplex vs duplex DNA selectivity, which shows that ligands **9a**−**i** and **15a**−**c**, and especially the para-substituted ligands **9a**−**h**, are significantly more G-quadruplex selective than BRACO-19. The lack of stabilization of a duplex DNA oligonucleotide complex ($\Delta T_{m,1\mu M} < 2.8$ °C) indicates a high level of selectivity for G-quadruplex forming sequences, which was confirmed by a competition assay using calf-thymus DNA at a 200-fold excess of duplex DNA. A subset of these ligands (**9a**−**c**) were assessed for duplex DNA interactions by SPR, with no significant duplex DNA interaction found ($K_A < 1.0 \times 10^3\ M^{-1}$). This represents at least 400- to 14000-fold selectivity for G-quadruplex vs duplex DNA. These selectivity results have been rationalized by the molecular modeling studies with ligands **9a**−**c** and duplex DNA, which show that the core of the ligands is sterically too large for intercalation. Although the ligands were observed to dock tightly into the duplex DNA grooves, these modes have lower calculated interaction energies relative to that for G-quadruplex interaction.

Examination of the predicted interaction energies for these ligands indicates a dependence upon the electrostatic contribution to the binding and an independence from the predicted binding mode, with all interaction energies comparable across this series.

Cell Biology. There are few clear patterns in the short term cell growth inhibtion data for the two cancer cell lines used here (IC_{50} values). However, it is apparent that altering the basic group from pyrrolidino (**9b**) as is the case for ligands **9g**−**i** results in improved MCF7 selectivity albeit with reduced potency. It is also evident that the linear ligands **10e** and **10f** have selectivity for cancer cells over a normal cell line and that the $n = 2$ side chain of **10e** confers enhanced potency. These effects do not correlate with the predicted G-quadruplex or duplex DNA $\Delta T_{m,1\mu M}$ results from the FRET assay. We have not measured cellular uptake of these compounds. However the potency shown by some compounds in the short term SRB cell viability assay (Table 5) indicates that some at least are readily able to cross cell membranes, although at this stage we cannot discount the possibility that the less potent ligands are not able to do so.

Investigation into the longer-term effects (1 week) of the more toxic ligands (for example, **9b**) in the MCF7 cell line used subcytotoxic concentrations of ligands. Over this period, the ligands had a significant effect on population growth, which was associated with a small induction of cellular senescence. No significant levels of telomere end−end fusions were observed over this time period. These results, taken with the lack of telomerase inhibitory activity, suggest that these ligands are at best only modest inducers of telomere uncapping/dysfunction. This further suggests that a minimum threshold level of telomeric quadruplex affinity is required for effective interference with telomere function in cancer cells, which is not reached by these particular diarylurea ligands but is achieved by compounds such as BRACO-19,[22,24,32,61,76] telomestatin,[20,56,62,63,67] and the more recently developed naphthalene diimides.[19]

There is a strong suggestion from the IC_{50} data that the compounds reported here fall into several distinct biological classes that may reflect distinct modes of action (though differences in cellular uptake cannot be discounted): (i) the para-substituted set **9a**−**c**/**g**−**i**, which are moderately selective for the cancer cell lines, especially MCF7; (ii) the smaller set **10a**−**f**, with compound **10e** showing exceptional selectivity; and (iii) the nonselective meta-substituted sets **9d**−**f** and **15a**−**c**. The diarylurea skeleton is represented in many kinase inhibitors, for example, multitargeted tyrosine kinase inhibitors[108] and inhibitors of insulin-like growth factor I receptor signaling.[109] Even though the substitution patterns in the present compounds have not been previously reported for kinase inhibitors, we cannot discount at present the possibility that the biologically active compounds reported here may be acting directly on kinase binding sites.

Conclusions

The purpose of this study was to design and evaluate a novel series of nonpolycyclic compounds that would show effective binding to quadruplex DNAs. This goal has been achieved through the diphenylurea-based scaffold. Even though initial studies of their cellular effects indicate that the derivatives discussed here do not show potent telomerase inhibitory activity, further analogue development is warranted. A number of the present compounds did show significant effects on cancer cell growth that are not associated with significant telomere uncapping/dysfunction and are unlikely to be effects on duplex DNA. We introduce the concept that a threshold level of quadruplex affinity is required for a compound to show such effects. It is also possible that interactions with nontelomeric quadruplexes may be involved, and screening is planned on larger libraries of derivatives with a more extensive set of quadruplexes from oncogenic promoter sequences,[37] as well as use of a larger panel of cancer cell lines.

Experimental Section

Fluorescence Resonance Energy Transfer (FRET) Assays. FRET oligonucleotides (Eurogentec Ltd., U.K.) have the following sequences: F21T, 5′FAM-d[$G_3(T_2AG_3)_3$]-TAMRA3′; *c-kit1*, 5′FAM-d[$AGAG_3AG_2GCGCTG_3AG_2AG_3GCT$]-TAMRA3′; *c-kit2*, 5′FAM-d[$C_3G_3CG_3CGCGAG_3AG_4AG_2$]-TAMRA3′;duplex,5′FAM-d[$(TA)_2GC(TA)_2T_6(TA)_2GC(TA)_2$]-TAMRA3′ where FAM is 6-carboxyfluoresein and TAMRA 6-carboxytetramethylrhodamine. For the FRET assay, the required oligonucleotide was suspended in FRET buffer (60 mM KCl, Kcacodylate, pH 7.4; 400 nM DNA) and heated to 85 °C for 10 min prior to cooling to room temperature. DNA was distributed (50 μL) across a 96-well RT-PCR plate (Bio-Rad) to which ligand was added (50 μL; stored as a 20 mM DMSO stock, −20 °C; diluted to 1 mM in HPLC grade DMSO) to afford the required concentration. FRET buffer was used as a negative control. DNA melting was assessed on a MJ Research Opticon DNA engine continuous fluorescence detector exciting at 450−495nm. Fluorescence values were recorded at 515−545nm at 0.5 °C intervals as the plate was heated from 30 to 100 °C. The data were analyzed with the Origin 7.0 software package (Origin Laboratory Corp., Northampton, MA). In the case of the *c-kit1* oligonucleotide, melting curves were fitted to sigmoid curves prior to analysis. The change in melting temperature at 1 μM ligand concentration ($\Delta T_{m,1\mu M}$) was calculated from four experiments by subtraction of the averaged negative control from the averaged 1 μM ligand melting temperature ± the maximum standard deviation (sd). For the competition assay, to F21T DNA (50 μL) was added calf thymus DNA (CT-DNA, 25 μL, 533.3 μM CT-DNA bp stock in 0.5 mM EDTA/30 mM K^+ cacodylate buffer) to afford the required CT-DNA bp concentration. To this was added ligand (25 μL, 4 μM) to afford the required ligand concentration (1 μM). FRET buffer represented no competitor. The percentage of retained stabilization was calculated from three experiments and normalized to the $\Delta T_{m,1\mu M}$ for that ligand with no CT-DNA competitor (100%) ± normalized sd. BRACO-19 was prepared in-house[30,32] to a HPLC purity of >98% (data not shown).

Circular Dchroism (CD) Sudies. CD spectra of the 24-mer telomeric DNA sequence d(TTAGGGTTAGGGTTAGGGTTAGGG) both in the absence of ligands and with ligands **9b**, **9d**, and **15b** together with two triazole-containing diarylurea derivatives synthesized in a separate project[110] were acquired on an Applied Photophysics Ltd. Chirascan spectrometer at King's College London. All samples were prepared at 100 μM in 100 mM potassium chloride/phosphate, pH 7.4, and heated to 95 °C and slowly annealed overnight to room temperature. The samples were further diluted with buffer to 0.8 optical density unit prior to data collection, and where appropriate, ligand was added to give a 1:1 molar ratio. UV absorbance and CD spectra were measured between 320 and 220 nm in a 10 mm path length cell. Spectra were recorded with a 0.5 nm step size, a 1.5 s time-per-point, and a spectral bandwidth of 1 nm. All spectra were acquired at room temperature, and buffer baseline was corrected. The concentration of the above oligonucleotide was determined by using the absorbance value at 260 nm and the Beer−Lambert law.

Surface Plasmon Resonance (SPR). Biosensor experiments were conducted in filtered, degassed HEPES buffer (10 mM HEPES, 100 mM KCl, 3 mM EDTA, 0.000 05 v/v of 10% P20 BIACORE surfactant, pH 7.3) at 25 °C. The 5′-biotin labeled DNA sequences (Integrated DNA Technologies) were HPLC purified and comprise the following sequences: hTel, 5′biotin-d[$AG_3(T_2AG_3)_3$]3′; *c-kit1*, 5′biotin-d[$(AG_3)_2CGCTG_3AG_2AG_3$]3′; *c-kit2*, 5′biotin-d[$(CG_3)_2$-$CGCGAG_3AG_4$]3′; *c-myc*, 5′biotin-d[$(AG_3TG_4)_2A$]3′; duplex, 5′biotin-d[$CGA_2T_2CGTCTC_2GA_2T_2CG$]3′. The experiments were conducted upon a BIAcore 2000 optical biosensor instrument (BIAcore Inc.). Flow cell 1 was left blank as a reference, while flow cells 2−4 were immobilized with DNA on a streptavidin-derivatized gold chip (SA chip from BIAcore) by manual injection of DNA stock solutions (flow rate of 1 μL/min) until the desired value of DNA response was obtained (350−400 RU). Typically, a series of different ligand concentrations (1 nM to 10 μM from 20 mM DMSO stock) were injected onto the chip (flow rate of 50 μL/min, 5−10 min) until a constant steady-state response was obtained followed by a dissociation period (buffer, 10 min). After every cycle, the chip surface was regenerated (20 s injection of 10 mM glycine solution, pH 2.0) followed by running buffer flow. The data were processed as previously described,[30,91] using BIAevaluation (BIAcore Inc.) and Kaleidagraph (Synergy Software) software for nonlinear least-squares optimization of the binding parameters.

Molecular Modeling. Molecular modeling was performed on an SGI Octane workstation (2 × 225 MHz MIPS R12000 CPUs; IRIX64 6.5 OS; Silicon Graphics Ltd.) with the Insight II software package (Accelerys Software Inc., 2000) utilizing the Builder, Discover, and Docking modules. G-Quadruplex DNA was prepared from the 22-mer crystal structure of the G-quadruplex formed from the human telomere of sequence d[$AG_3(T_2AG_3)_3$] (PDB 1KF1),[68]

and a self-complementary duplex DNA was built in Insight II from the sequence d[$(TA)_2GC(TA)_2$]. An intercalation site with 6.76 Å base-pair separation was introduced at the GC step of the DNA duplex. Ligands were built with atomic potentials and partial charges assigned in the CVFF force field prior to minimization (500 steps steepest descents; 5000 steps conjugate gradients; rmsd of 0.001 kcal mol^{-1} $Å^{-1}$) in the Discover module. Basic side chains consisting of the pyrrolidino, dimethylamino, and piperidino groups were built as protonated species by addition of a formal atomic charge. Morpholino groups were kept uncharged. Core conformational analysis was achieved by manual rotation prior to minimization (500 steps steepest descent; successive 2000 step conjugate gradients until convergence to an rmsd of 0.01 kcal mol^{-1} $Å^{-1}$) in the Discover module of Insight II.

A multistage Monte Carlo minimization simulated-annealing docking protocol analogous to those previously reported[94,95] was utilized in the Docking module of Insight II to determine the potential low energy ligand−DNA complexes and their energy, using default program settings unless specified. For G-quadruplex interaction, the ligand was positioned ∼5 Å above the center of the 3′-G-quartet, defining their hydrogen atoms as the binding site about which a Monte Carlo minimization methodology was employed to generate 200 random orientations of the starting structure, with van der Waals radii scaled to 10% of their full values and charges not considered. The maximum allowable energy change of successive random structures was 10 000 kcal mol^{-1} with an energy range of 40 kcal mol^{-1}. Each conformation was minimized (300 steps of conjugate gradients), and the 75 lowest total system energy conformations were filtered by Insight II for further analysis. For duplex DNA interaction, an analogous procedure was used defining the binding site as all of the hydrogen atoms that project into the required DNA groove or by inserting the ligand into the DNA pseudointercalation site in the best perceived conformation, defining the hydrogen atoms of the GC base pairs as the binding site. These 75 structures were subjected to 800 steps of conjugate gradients minimization in which charges were included, van der Waals radii were set to 100%, and the distant dependent dielectric constant was 1*r*, prior to simulated annealing between 500 and 300 K over 10 ps to the predefined binding site. The resulting structures were energy-minimized (800 steps of conjugate gradients) and the 25 lowest total system energy conformations filtered by Insight II for further manual evaluation. These docked structures were analyzed on the basis of the chemical correctness of the ligand ensuring trans urea and amide integrity, the lowest total interaction energy of the complex assessed for all atoms with no cutoff, the number of hydrogen bonding interactions observed, the binding modes that best represent the populations, and the perceived correctness of the proposed ligand binding mode. This allowed the selection of two lead low energy binding conformations for further analysis. Each low energy binding conformation was used to define a flexible binding site containing all DNA atoms residing 7−8 Å from the ligand, fixing all other atoms and tethering the 3′-G-quartet or the terminal duplex DNA TA base pairs. A further 30 rounds of (300 steps of conjugate gradients minimization prior to simulated annealing between 800 and 200 K over 10 ps) were performed using a distance-dependent dielectric constant of 4*r*. Final minimization (1000 steps conjugate gradients) allowed the filtering of the 15 lowest total system energy conformations by Insight II for final analysis. These bound ligand−DNA complexes were manually assessed by the predefined criteria, averaging the total interaction energy observed for the 10 lowest energy binding conformations ± sd, assessed between all atoms with no cutoff. Figures were constructed from a docked binding conformation selected to best represent the optimal low energy binding conformations of the population.

Cell Culture. Cell lines were supplied by ATCC-LGC Promochem and viability maintained in a Heraeus Hera Cell 240 incubator (37 °C, 5% CO_2, 75 cm^2 plates, TPP). Cells were removed for experimentation as required. Sterile work was conducted in a Heraeus Hera Safe hood. Dulbecco's modified Eagles medium (DMEM, Invitrogen) supplemented with fetal bovine serum (10% v/v, Invitrogen), hydrocortisone (0.5 μg/mL, Acros Organics), L-glutamine (2 mM, Invitrogen), and nonessential amino acids (1×, Invitrogen) was used for the MCF7 and A549 cell lines, and minimum essential medium (MEM; Sigma-Aldrich) supplemented with fetal bovine serum (10% v/v, Invitrogen), L-glutamine (2 mM, Invitrogen), and nonessential amino acids (1×, Invitrogen) was used for the WI38 cell line.

SRB Cytotoxicity Assay. Short-term growth inhibition was measured using the SRB assay as described previously.[22,30,100] Briefly, cells were seeded (4000 cells/wells) into the wells of 96-well plates in appropriate medium and incubated overnight to allow the cells to attach. Subsequently cells were exposed to freshly made solutions of drug at increasing concentrations between 0.25 and 50 μM in quadruplicate and incubated for a further 96 h. Following this the cells were fixed with ice cold trichloacetic acid (10% w/v) for 30 min and stained with 0.4% SRB dissolved in 1% acetic acid for 15 min. All incubations were carried out at room temperature. The IC_{50} value, concentration required to inhibit cell growth by 50%, was determined from the mean absorbance at 540 nm for each drug concentration expressed as a percentage of the well absorbance in untreated control cells.

Subcytotoxic Induction of Cellular Senescence (β-Galactosidase Assay).[30,101] MCF7 cells (1×10^5, 10 mL of media, ATCC-LGC Promochem) were exposed to two independent subcytotoxic concentrations of the required ligand over a 1 week period, with a biweekly treatment. A media negative control was also screened. Cells were counted on a Neybauer hemocytometer (Assistant, Germany) and the number of cellular population doublings assessed by the equation $n = (\log P_n - \log P_0)/\log 2$ where P_n is the number of cells collected and P_0 the initial seeding density. Cells were stained for senescence using the β-galactosidase staining kit (Cell Signaling Technology) according to the manufacturer's instructions. In short, cells were seeded (1×10^5, 2 mL) in a 6-well plate (Fisher-Scientific) with the required ligand concentration and incubated overnight. The medium was removed and the well washed with PBS (2 mL) prior to fixing (1× fixative solution, 10 min). The fixative was removed and the well washed with PBS (2 × 2 mL) prior to the addition of the staining solution (1 mL), and the plates were incubated overnight. Three independent fields of cells were visualized (200× magnification) from both repeats, with the mean percentage of blue senescent cells reported ± sd.

TRAP-LIG Assay. This was performed as recently described.[98]

Chemistry. All reagents were reagent grade and were used as supplied without further purification (Sigma-Aldrich, Alfa Aesar, Avocado Organics, and Lancaster Synthesis). Palladium catalyst was 10 wt % loading on activated carbon. Ammonia in methanol (NH_3/MeOH, ∼7 N; Sigma-Aldrich) was diluted in MeOH as required. Solvents (BDH and Fisher Scientific), anhydrous solvents (Sigma-Aldrich), and HPLC grade solvents (Fisher Scientific) were used as supplied. Microwave reactions were conducted in a Biotage initiator microwave, software version 1.1, in Biotage vials (0.5−2.0 or 2.0−5.0 mL) sealed with Biotage caps with septa. All chemistry was conducted in clean, oven-dried glassware. ^1H and ^{13}C NMR spectra were recorded at 295 K on on a Bruker Avance 400 spectrometer using the specified deuterated solvent (GOSS Scientific and Sigma-Aldrich). NMR spectra were analyzed by the MestReC 4.5.6.0 program with chemical shifts calibrated to the residual proton and carbon resonance of the solvent. NMR multiplicity and coupling constants (*J*) are reported as observed. Melting points (mp) were measured on a Bibby Stuart Scientific SMP3 melting point apparatus, where "dec" indicates decomposition. Mass spectra were recorded on a ThermoQuest Navigator mass spectrometer using electrospray ionization in positive ($[M + H]^+$) or negative ($[M - H]^-$) modes. High resolution accurate mass spectra were recorded on a Micromass Q-TTOF Ultima Global tandem mass spectrometer using electrospray ionization mode and 50% acetonitrile in water and 0.1% FA as solvent and processed using the MassLab 3.2 software. Infrared spectra were recorded from neat samples on a Nicolet Smart Golden Gate spectrometer (Avatar 360 FT-IR E.S.P.) and processed using the software package OMNIC ESP 5.1. Flash chromatography was conducted on silica gel (partial size 33−70

μm, BDH). Analytical HPLC was performed on a Gilson chromatograph with a YMC C18 5 μm (100 mm × 4.6 mm) column and an Agilent 1100 series photodiode array detector. Spectra were processed in the Unipoint 5.11 software, and compound purity and retention times (t_R) were assessed at 254 nm unless stated otherwise. Several HPLC solvent systems and gradients were employed as specified: method A, 0.1% TFA in MeOH and 0.1% aqueous TFA, 25−75% organic over 28 min (1 mL/min); method B, 0.1% TFA in MeOH and 0.1% aqueous TFA, 25−50% organic over 18 min (1 mL/min); method C, 0.1% FA in acetonitrile and 0.1% aqueous FA, 5−50% organic over 28 min (1 mL/min); method D, 0.1% FA in acetonitrile and 0.1% aqueous FA, 5−50% organic over 18 min (1 mL/min); method E, 0.1% FA in MeOH and 0.1% aqueous FA, 25−75% organic over 18 min (1 mL/min). Semipreparative reversed-phase HPLC (semiprep HPLC) was performed on a Gilson chromatograph with a Gilson 215 liquid handler, a Gilson 845Z injection module coupled to a Gilson UV/visible 155 detector, and a YMC C18 5 μm (100 mm × 20 mm) column. Several HPLC solvent systems, gradients, and methods of sample isolation were employed as specified: method F, 0.1% TFA in MeOH and 0.1% aqueous TFA, 25−75% organic over 25 min (10 mL/min), injected from 25% MeOH in 0.1% aqueous TFA (3 mL); method G, 0.1% TFA in MeOH and 0.1% aqueous TFA, 25−50% organic over 60 min, 50−75% organic over 5 min (10 mL/min), injected from 25% MeOH in 0.1% aqueous TFA (3 mL). Purified compounds were isolated by reduction of fraction volumes (5 mL), precipitation with 5% NH_3 (aq), and filtration.

Method 1 (1a−f and 12a−c). (a) The required nitroaniline was dissolved in THF (150 mL) and cooled to 0 °C prior to the addition of TEA (2 equiv) and the required acid chloride (1.5−2 equiv), and the mixture stirred overnight at room temperature. The precipitate was filtered and the solvent evaporated in vacuo. The product was either precipitated with saturated $NaHCO_3$ (aq) (200 mL) or dissolved in EtOAc (50 mL), washed with 5% NH_3 (aq) (50 mL), brine (50 mL), and dried over $MgSO_4$. (b) The required nitroaniline (15.0 g, 0.109 mol) was added to the appropriate acid chloride (45 mL, 0.402−0.471 mol) in portions at room temperature, followed by stirring at 50 °C overnight. The mixture was cooled to 0 °C and the product isolated by filtration, washing with ether (50 mL).

Method 2 (2a−i and 13a−c). 1a,**b/d−e/g−i** or **12a−c** were dissolved in MeOH/THF (5−100 mL), and the required amine base (2−3.6 equiv) was added. The mixture was either (a) stirred overnight at room temperature prior to the solvent being removed (5% NH_3 (aq) (50 mL) was added and the product extracted with EtOAc (50 mL), washed with brine (25 mL), and dried over $MgSO_4$), (b) heated under reflux for 4 h prior to workup as above, or (c) stirred at 30 °C overnight prior to workup as above. **1c/f** was reacted with neat pyrrolidine (20 mL, 0.240 mol) at room temperature overnight, followed by evaporation of the excess pyrrolidine and workup as described above.

Method 3 (3a−i and 14a−c). (a) **2a−i** were dissolved in MeOH (100 mL), and then ammonium formate (10 equiv) and Pd/C (0.1 equiv w/w) were added. The mixture was stirred overnight at room temperature prior to filtration through Celite and evaporation of the solvent. The residue was dissolved in $CHCl_3$ (100 mL), washed with 5% NH_3 (aq) (2 × 50 mL), brine (50 mL), and dried over $MgSO_4$. (b) **13a−c** were suspended in absolute EtOH (4 mL) prior to the addition of ammonium formate (4 equiv) and Pd/C (0.1 equiv w/w). The mixture was heated by microwave irradiation (120 °C, 10 min, 7 bar) followed by workup as described above.

Method 4 (4j,k,l). The required nitrobenzoic acid (5.0 g, 0.030 mol) was dissolved in anhydrous DCM (150 mL), and DMF was added as required. DMAP (500 mg, 0.1 equiv w/w) and ^{t}BuOH (4.29 mL, 0.045 mol, 1.5 equiv) were added prior to cooling the mixture to 0 °C and adding DCC (6.79 g, 0.033 mol, 1.1 equiv) in two portions. The mixture was warmed to room temperature and stirred for 4 h. The precipitate was filtered and the DCM washed with 1 M HCl (aq) (2 × 50 mL), brine (50 mL) and dried over $MgSO_4$. The resulting oil was purified by flash chromatography.

Method 5 (5j,k). 4j,**k** were dissolved in MeOH (100 mL), and Pd/C (0.1 equiv w/w) was added prior to purging with H_2 (g), and the mixture was stirred at room temperature until reaction was complete, when it was filtered through Celite and the solvent evaporated in vacuo.

Method 6 (6j,k and 15a−c). (a) **5j**,**k** were dissolved in anhydrous THF to a concentration of 0.4 M, and CDI (0.6−1.2 equiv) was added. The mixture was heated at reflux for 24 h under N_2 (g). The THF was evaporated and the residue dissolved in EtOAc (200 mL), washed with 1 M HCl (aq) (2 × 100 mL), brine (50 mL), and dried over $MgSO_4$. (b) As above, **14a−c** were reacted with CDI (1.0 equiv) by microwave irradiation (75 °C, 20 min, N_2 (g)). The mixture was cooled to 0 °C and the product precipitated with EtOAc (10 mL).

Method 7 (7j,k). 6j,**k** were suspended in TFA (30 mL) and stirred vigorously at room temperature for 1 h. The precipitate was isolated by filtration, washed with DCM (50 mL), and oven-dried. If no precipitate formed, precipitation was induced by cooling the mixture to 0 °C and treatment with ether (50 mL).

Method 8 (8a−f, 9a−i, and 10a−f). 7j,**k** were dissolved in anhydrous DMF (8 mL), and to this were added the required side chains **3a−i** (4 equiv) and PyBOP (3 equiv). The mixture was stirred at room temperature under N_2 (g) for 22 h. The DMF was evaporated and the resulting oil suspended in $CHCl_3$ (20 mL) with sonication. The resulting precipitate was isolated by filtration; however, when an oily residue formed, the organic solvent was decanted. In either instance, this crude material was dissolved in NH_3/MeOH (1 M, 3 mL), and the product was precipitated with 5% NH_3 (aq) (30 mL) and isolated by filtration.

Detailed experimental procedures and analytical data for the side chain building blocks **1a−f**, **2a−i**, **3a-i**, **4j−l**, **5j−l** and the quinazoline dione ligands **8a−f** are given in the Supporting Information.

2,2′-Ureylene-di-(*tert*-Butylbenzoate) (6j). Following method 6a, **5j** (3.38 g, 17.488 mmol) was reacted with CDI (3.40 g, 20.986 mmol) to yield a yellow solid (3.59 g, 8.703 mmol, quant) which was used without further purification. ^{1}H NMR (400 MHz, $CDCl_3$) 10.69 (2H, s), 8.46 (2H, dd, J = 8.5, 0.9 Hz), 7.96 (2H, dd, J = 8.0, 1.6 Hz), 7.49 (2H, ddd, J = 8.7, 7.3, 1.7 Hz), 6.99 (2H, ddd, J = 8.2, 7.3, 1.1 Hz), 1.64 (18H, s) ppm. ^{13}C NMR (100 MHz, $CDCl_3$) 167.8, 152.4, 142.4, 133.8, 131.0, 121.1, 120.0, 116.4, 82.3, 28.3 ppm. HRMS m/z calcd $C_{23}H_{28}N_2O_5$ $[M + H]^+$ 413.2071, found 413.2065.

3,3′-Ureylene-di-(*tert*-butyl benzoate) (6k). Following method 6a, **5k** (4.01 g, 20.744 mmol) was reacted with CDI (2.02 g, 12.458 mmol) to yield a white solid (3.97 g, 9.625 mmol, 93%). Mp 296 °C dec. ^{1}H NMR (400 MHz, DMSO-d_6) δ 8.97 (2H, s), 8.09 (2H, t, J = 1.8 Hz), 7.75 (2H, ddd, J = 8.0, 2.1, 1.0 Hz), 7.58 (2H, d, J = 7.8 Hz), 7.46 (2H, t, J = 7.9 Hz), 1.61 (18H, s) ppm. ^{13}C NMR (100 MHz, DMSO- d_6) δ 164.8, 152.5, 139.8, 131.9, 129.0, 122.5, 122.5, 118.7, 80.7, 27.8 ppm. HRMS m/z calcd $C_{23}H_{28}N_2O_5$ $[M + H]^+$ 413.2071, found 413.2075.

4,4′-Ureylene-di-(*tert*-butyl benzoate) (6l). Following method 6a, **5l** (3.71 g, 19.202 mmol) was reacted with CDI (3.74 g, 23.042 mmol) to yield a white solid (3.94 g, 9.552 mmol, 99%) which was used without further purification. ^{1}H NMR (400 MHz, $CDCl_3$) δ 9.23 (2H, s), 7.89 (4H, d, J = 8.8 Hz), 7.63 (4H, d, J = 8.8 Hz), 1.59 (18H, s) ppm. HRMS m/z calcd $C_{23}H_{28}N_2O_5$ $[M + H]^+$ 413.2071, found 413.2092.

2,2′-Ureylenedibenzoic Acid (7j). Following method 7, **6j** (3.11 g, 7.546 mmol) was deprotected to yield a white solid (1.05 g, 3.483 mmol, 46%). Mp 192−194 °C. ^{1}H NMR (400 MHz, DMSO-d_6) 13.48 (2H, s), 10.73 (2H, s), 8.29 (2H, dd, J = 8.4, 0.8 Hz), 7.95 (2H, dd, J = 7.9, 1.6 Hz), 7.56 (2H, ddd, J = 8.7, 7.3, 1.7 Hz), 7.09 (2H, m) ppm. ^{13}C NMR (100 MHz, DMSO- d_6) 169.7, 151.7, 141.6, 133.8, 131.0, 121.5, 119.7, 116.4 ppm. HRMS m/z calcd $C_{15}H_{12}N_2O_5$ $[M + H]^+$ 301.0819, found 301.0814.

3,3′-Ureylenedibenzoic Acid (7k). Following method 7, **6k** (3.01 g, 7.266 mmol) was deprotected to yield a white solid (2.18 g, 7.260 mmol, quant). Mp 321−323 °C. ^{1}H NMR (400 MHz, DMSO-d_6) δ 12.84 (2H, s), 8.97 (2H, s), 8.15 (2H, t, J = 1.7 Hz), 7.66

(2H, ddd, J = 8.1, 2.0, 0.9 Hz), 7.57 (2H, d, J = 7.8 Hz), 7.41 (2H, t, J = 7.9 Hz) ppm. ^{13}C NMR (100 MHz, DMSO- d_6) δ 167.2, 152.5, 139.8, 131.3, 129.0, 122.8, 122.5, 119.0 ppm. HRMS m/z calcd $C_{15}H_{12}N_2O_5$ $[M + H]^+$ 301.0819, found 301.0807.

4,4′-Ureylenedibenzoic Acid (7l). Following method 7, **6l** (3.12 g, 7.558 mmol) was deprotected to yield a fine white powder (2.15 g, 7.172 mmol, 95%). Mp >350 °C [lit. >400 °C]. ^{1}H NMR (400 MHz, DMSO) δ 12.62 (2H, s), 9.21 (2H, s), 7.88 (4H, d, J = 8.7 Hz), 7.58 (4H, d, J = 8.7 Hz) ppm. ^{13}C NMR (100 MHz, DMSO- d_6) δ 166.9, 151.9, 143.6, 130.5, 123.9, 117.3 ppm. HRMS m/z calcd $C_{15}H_{12}N_2O_5$ $[M + H]^+$ 301.0819, found 301.0817.

1,3-Bis(3-(4-(2-(pyrrolidin-1-yl)acetamido)phenylcarbamoyl)phenyl)urea (9a). Following method 8, **7k** (150.0 mg, 0.500 mmol) was reacted with **3a** (438.1 mg, 1.998 mmol) to yield a pale-brown solid (333.0 mg, 0.474 mmol, 95%), which was purified by semiprep HPLC (method F). HPLC (method A) 97%, t_R = 17.69 min. Mp 286−288 °C. ^{1}H NMR (400 MHz, DMSO- d_6) δ 10.20 (2H, s), 9.73 (2H, s), 8.98 (2H, s), 7.98 (2H, s), 7.70 (6H, d, J = 8.9 Hz), 7.61 (4H, d, J = 8.9 Hz), 7.56 (2H, d, J = 7.8 Hz), 7.44 (2H, t, J = 7.9 Hz), 3.32 (4H, s), 2.67 (8H, m), 1.77 (8H, m) ppm. ^{13}C NMR (100 MHz, DMSO- d_6) δ 167.9, 165.2, 152.4, 139.7, 135.7, 134.6, 134.3, 128.6, 121.1, 120.8, 120.6, 119.6, 117.6, 59.0, 53.7, 23.3 ppm. HRMS m/z calcd $C_{39}H_{42}N_8O_5$ $[M + H]^+$ 703.3351, found 703.3386.

1,3-Bis(3-(4-(3-(pyrrolidin-1-yl)propanamido)phenylcarbamoyl)phenyl)urea (9b). Following method 8, **7k** (150.0 mg, 0.500 mmol) was reacted with **3b** (466.2 mg, 1.998 mmol) to yield a white solid (346.0 mg, 0.473 mmol, 95%). HPLC (method A) 98%, t_R = 19.00 min. Mp 330 °C dec. ^{1}H NMR (400 MHz, DMSO-d_6) δ 10.18 (2H, s), 10.05 (2H, s), 8.95 (2H, s), 7.97 (2H, s), 7.70 (6H, m), 7.55 (6H, m), 7.44 (2H, t, J = 7.9 Hz), 2.75 (4H, t, J = 7.1 Hz), 2.50 (12H, m), 1.70 (8H, m) ppm. ^{13}C NMR (100 MHz, DMSO- d_6) δ 169.6, 165.2, 152.4, 139.6, 135.7, 135.0, 134.3, 128.7, 121.1, 120.8, 120.7, 119.1, 117.6, 53.3, 51.4, 35.7, 23.0 ppm. HRMS m/z calcd $C_{41}H_{46}N_8O_5$ $[M + H]^+$ 731.3664, found 731.3690.

1,3-Bis(3-(4-(4-(pyrrolidin-1-yl)butanamido)phenylcarbamoyl)phenyl)urea (9c). Following method 8, **7k** (150.0 mg, 0.500 mmol) was reacted with **3c** (494.2 mg, 1.998 mmol) to yield a white solid (344.8 mg, 0.454 mmol, 91%). HPLC (method A) 96%, t_R = 19.86 min. Mp 239−241 °C. ^{1}H NMR (400 MHz, DMSO- d_6) δ 10.20 (2H, s), 9.89 (2H, s), 9.00 (2H, s), 7.99 (2H, s), 7.70 (6H, m), 7.57 (6H, m), 7.44 (2H, t, J = 7.9 Hz), 2.50 (12H, m), 2.35 (4H, t, J = 7.4 Hz), 1.77 (4H, m), 1.70 (8H, m) ppm. ^{13}C NMR (100 MHz, DMSO- d_6) δ 170.7, 165.2, 152.4, 139.7, 135.7, 135.1, 134.2, 128.6, 121.1, 120.8, 120.6, 119.1, 117.6, 54.9, 53.4, 45.7, 34.1, 23.0 ppm. HRMS m/z calcd $C_{43}H_{50}N_8O_5$ $[M + H]^+$ 759.3977, found 759.3940.

1,3-Bis(3-(3-(2-(pyrrolidin-1-yl)acetamido)phenylcarbamoyl)phenyl)urea (9d). Following method 8, **7k** (150.0 mg, 0.500 mmol) was reacted with **3c** (438.1 mg, 1.998 mmol) to yield a pale-yellow solid (310.1 mg, 0.441 mmol, 88%). HPLC (method A) 91%, t_R = 18.69 min. Mp 154−157 °C. ^{1}H NMR (400 MHz, DMSO- d_6) δ 10.27 (2H, s), 9.78 (2H, s), 8.96 (2H, s), 8.12 (2H, s), 7.79 (2H, s), 7.71 (2H, d, J = 8.0 Hz), 7.57 (2H, d, J = 7.7 Hz), 7.44 (4H, m), 7.38 (2H, d, J = 8.3 Hz), 7.26 (2H, t, J = 8.0 Hz), 3.31 (4H, s), 2.65 (8H, m), 1.76 (8H, m) ppm. ^{13}C NMR (100 MHz, DMSO- d_6) δ 168.3, 165.6, 152.6, 139.7, 139.4, 138.8, 135.8, 128.8, 128.7, 121.3, 121.0, 117.8, 115.7, 115.0, 111.8, 59.2, 53.7, 23.4 ppm. HRMS m/z calcd $C_{39}H_{42}N_8O_5$ $[M + H]^+$ 703.3351, found 703.3344.

1,3-Bis(3-(3-(3-(pyrrolidin-1-yl)propanamido)phenylcarbamoyl)phenyl)urea (9e). Following method 8, **7k** (150.0 mg, 0.500 mmol) was reacted with **3e** (466.2 mg, 1.998 mmol) to yield a pale-yellow solid (292.4 mg, 0.400 mmol, 80%). HPLC (method A) 93%, t_R = 19.39 min. Mp 160 − 163 °C. ^{1}H NMR (400 MHz, DMSO- d_6) δ 10.26 (2H, s), 10.13 (2H, s), 9.00 (2H, s), 8.10 (2H, s), 7.98 (2H, s), 7.72 (2H, d, J = 7.9 Hz), 7.57 (2H, d, J = 7.7 Hz), 7.44 (4H, m), 7.38 (2H, d, J = 7.9 Hz), 7.25 (2H, t, J = 7.7 Hz), 2.72 (4H, t, J = 6.9 Hz), 2.49 (12H, m), 1.70 (8H, m) ppm. ^{13}C NMR (100 MHz, DMSO- d_6) δ 170.0, 165.5, 152.6, 139.6, 139.3, 139.3, 135.7, 128.6, 128.5, 121.2, 120.9, 117.7, 115.2, 114.5, 111.2, 53.3, 51.4, 35.9, 23.1 ppm. HRMS m/z calcd $C_{41}H_{46}N_8O_5$ $[M + H]^+$ 731.3664, found 731.3651.

1,3-Bis(3-(3-(4-(pyrrolidin-1-yl)butanamido)phenylcarbamoyl)phenyl)urea (9f). Following method 8, **7k** (150.0 mg, 0.500 mmol) was reacted with **3f** (494.2 mg, 1.998 mmol) to yield a white solid (189.6 mg, 0.249 mmol, 50%). HPLC (method A) 96%, t_R = 19.56 min. Mp 234−236 °C. ^{1}H NMR (400 MHz, DMSO- d_6) δ 10.26 (2H, s), 9.94 (2H, s), 9.01 (2H, s), 8.11 (2H, s), 7.99 (2H, s), 7.72 (2H, d, J = 8.0 Hz), 7.57 (2H, d, J = 7.6 Hz), 7.43 (4H, m), 7.37 (2H, d, J = 7.9 Hz), 7.25 (2H, t, J = 8.1 Hz), 2.48 (12H, m), 2.37 (4H, t, J = 7.3 Hz), 1.77 (4H, m), 1.69 (8H, m) ppm. ^{13}C NMR (100 MHz, DMSO- d_6) δ 171.0, 165.5, 152.5, 139.6, 139.4, 139.3, 135.7, 128.6, 128.5, 121.2, 120.9, 117.7, 115.1, 114.5, 111.3, 54.9, 53.4, 34.2, 24.1, 23.0 ppm. HRMS m/z calcd $C_{43}H_{50}N_8O_5$ $[M + H]^+$ 759.3977, found 759.3942.

1,3-Bis(3-(4-(3-(dimethylamino)propanamido)phenylcarbamoyl)phenyl)urea (9g). Following method 8, **7k** (100.0 mg, 0.333 mmol) was reacted with **3g** (276.1 mg, 1.333 mmol) to yield a white solid (222.8 mg, 0.328 mmol, 99%), which was purified by filtration from boiling MeOH (2 mL). HPLC (method C) 95%, t_R = 17.28 min. Mp 322 −324 °C. ^{1}H NMR (400 MHz, DMSO- d_6) δ 10.18 (2H, s), 10.00 (2H, s), 8.94 (2H, s), 7.98 (2H, s), 7.70 (6H, m), 7.56 (6H, m), 7.44 (2H, t, J = 7.9 Hz), 2.57 (4H, t, J = 7.0 Hz), 2.44 (4H, t, J = 6.9 Hz), 2.19 (12H, s) ppm. ^{13}C NMR (100 MHz, DMSO- d_6) δ 169.9, 165.3, 152.5, 139.7, 135.8, 135.1, 134.4, 128.8, 121.2, 120.9, 120.7, 119.2, 117.7, 55.1, 44.9, 34.7 ppm. HRMS m/z calcd $C_{37}H_{42}N_8O_5$ $[M + H]^+$ 679.3351, found 679.3334.

1,3-Bis(3-(4-(3-(piperidin-1-yl)propanamido)phenylcarbamoyl)phenyl)urea (9h). Following method 8, **7k** (100.0 mg, 0.333 mmol) was reacted with **3h** (329.8 mg, 1.333 mmol) to yield a white solid (221.1 mg, 0.291 mmol, 87%), which was purified by filtration from boiling MeOH (2 mL). HPLC (method C) 100%, t_R = 18.71 min. Mp 322−324 °C. ^{1}H NMR (400 MHz, DMSO- d_6) δ 10.18 (2H, s), 10.14 (2H, s), 8.95 (2H, s), 7.97 (2H, s), 7.70 (6H, m), 7.55 (6H, m), 7.44 (2H, t, J = 7.9 Hz), 2.60 (4H, t, J = 7.0 Hz), 2.45 (4H, t, J = 7.0 Hz), 2.39 (8H, m), 1.51 (8H, m), 1.40 (4H, m) ppm. ^{13}C NMR (100 MHz, DMSO- d_6) δ 167.0, 165.3, 152.5, 139.7, 135.8, 135.1, 134.4, 128.7, 121.2, 120.9, 120.8, 119.2, 117.7, 54.4, 53.6, 34.0, 25.6, 24.0 ppm. HRMS m/z calcd $C_{43}H_{50}N_8O_5$ $[M + 2H]^{+2}$ 380.2025, found 380.2018.

1,3-Bis(3-(4-(3-(morpholino)propanamido)phenylcarbamoyl)phenyl)urea (9i). Following method 8, **7k** (100.0 mg, 0.333 mmol) was reacted with **3i** (332.4 mg, 1.333 mmol) to yield a pale-purple solid (239.2 mg, 0.314 mmol, 94%), which was purified by filtration from boiling MeOH (2 mL). HPLC (method C) 97%, t_R = 17.20 min. Mp 313−315 °C. ^{1}H NMR (400 MHz, DMSO- d_6) δ 10.19 (2H, s), 10.00 (2H, s), 8.92 (2H, s), 7.98 (2H, s), 7.70 (6H, m), 7.56 (6H, m), 7.44 (2H, t, J = 7.9 Hz), 3.59 (8H, t, J = 4.5 Hz), 2.64 (4H, t, J = 7.0 Hz), 2.48 (4H, t, J = 7.1 Hz), 2.42 (8H, m) ppm. ^{13}C NMR (100 MHz, DMSO- d_6) δ 169.8, 165.3, 152.5, 139.7, 135.8, 135.1, 134.4, 128.8, 121.2, 120.9, 120.8, 119.2, 117.7, 66.2, 54.2, 53.0, 33.8 ppm. HRMS m/z calcd $C_{41}H_{46}N_8O_7$ $[M + H]^+$ 763.3562, found 763.3539.

1,3-Bis(4-(4-(2-(pyrrolidin-1-yl)acetamido)phenylcarbamoyl)phenyl)urea (10a). Following method 8, **7l** (150.0 mg, 0.500 mmol) was reacted with **3a** (438.1 mg, 1.998 mmol) to yield a dark-brown solid (325.3 mg, 0.463 mmol, 93%), which was purified by semiprep HPLC (method F). HPLC (method A, 280nm) 98%, t_R = 19.23 min. Mp 296−298 °C. ^{1}H NMR (400 MHz, DMSO- d_6) δ 10.04 (2H, s), 9.65 (2H, s), 9.14 (2H, s), 7.94 (4H, d, J = 8.8 Hz), 7.69 (4H, d, J = 9.0 Hz), 7.61 (4H, d, J = 8.8 Hz), 7.60 (4H, d, J = 9.0 Hz), 3.25 (4H, s), 2.61 (8H, m), 1.76 (8H, m) ppm. HRMS m/z calcd $C_{39}H_{42}N_8O_5$ $[M + H]^+$ 703.3351, found 703.3353.

1,3-Bis(4-(4-(3-(pyrrolidin-1-yl)propanamido)phenylcarbamoyl)phenyl)urea (10b). Following method 8, **7l** (150.0 mg, 0.500 mmol) was reacted with **3b** (466.2 mg, 1.998 mmol) to yield an off-white solid (298.6 mg, 0.409 mmol, 82%). HPLC (method A, 280nm) 99%, t_R = 18.65 min. Mp 299−301 °C. ^{1}H NMR (400 MHz, DMSO- d_6) δ 10.04 (4H, s), 9.15 (2H, s), 7.94 (4H, d, J = 8.6 Hz), 7.69 (4H, d, J = 8.8 Hz), 7.62 (4H, d, J = 8.6 Hz), 7.55 (4H, d, J = 8.8 Hz), 2.77 (4H, t, J = 6.4 Hz), 2.50 (12H, m), 1.72

(8H, m) ppm. HRMS *m/z* calcd $C_{41}H_{46}N_8O_5$ $[M + H]^+$ 731.3664, found 731.3653.

1,3-Bis(4-(4-(4-(pyrrolidin-1-yl)butanamido)phenylcarbamoyl)phenyl)urea (10c). Following method 8, **7l** (150.0 mg, 0.500 mmol) was reacted with **3c** (494.2 mg, 1.998 mmol) to yield a brown crystalline solid (332.3 mg, 0.438 mmol, 88%). HPLC (method A, 280nm) 91%, t_R = 20.01 min. Mp 289−291 °C.^{1}H NMR (400 MHz, DMSO-d_6) δ 10.02 (2H, s), 9.85 (2H, s), 9.16 (2H, s), 7.93 (4H, d, J = 8.7 Hz), 7.67 (4H, d, J = 8.9 Hz), 7.61 (4H, d, J = 8.7 Hz), 7.55 (4H, d, J = 8.9 Hz), 2.5 (12H, m), 2.35 (4H, t, J = 7.3 Hz), 1.77 (4H, m), 1.69 (8H, m) ppm. HRMS *m/z* calcd $C_{43}H_{50}N_8O_5$ $[M + H]^+$ 759.3977, found 759.3992.

1,3-Bis(4-(3-(2-(pyrrolidin-1-yl)acetamido)phenylcarbamoyl)phenyl)urea (10d). Following method 8, **7l** (150.0 mg, 0.500 mmol) was reacted with **3d** (438.1 mg, 1.998 mmol) to yield a pale-yellow solid (265.0 mg, 0.377 mmol, 75%), which was purified by semiprep HPLC (method F). HPLC (method A) 99%, t_R = 18.35 min. Mp 232−234 °C. ^{1}H NMR (400 MHz, DMSO-d_6) δ 10.10 (2H, s), 9.71 (2H, s), 9.15 (2H, s), 8.11 (2H, s), 7.95 (4H, d, J = 8.8 Hz), 7.62 (4H, d, J = 8.8 Hz), 7.46 (2H, d, J = 8.2 Hz), 7.36 (2H, d, J = 8.5 Hz), 7.25 (2H, t, J = 8.1 Hz), 3.28 (4H, s), 2.63 (8H, m), 1.76 (8H, m) ppm. ^{13}C NMR (100 MHz, DMSO- d_6) δ 168.5, 164.8, 152.1, 142.6, 139.5, 138.7, 128.8, 128.6, 127.9, 117.2, 115.6, 114.7, 111.7, 59.3, 53.6, 23.4 ppm. HRMS *m/z* calcd $C_{39}H_{42}N_8O_5$ $[M + H]^+$ 703.3351, found 703.3375.

1,3-Bis(4-(3-(3-(pyrrolidin-1-yl)propanamido)phenylcarbamoyl)phenyl)urea (10e). Following method 8, **7l** (150.0 mg, 0.500 mmol) was reacted with **3e** (466.2 mg, 1.998 mmol) to yield a pale-yellow solid (233.1 mg, 0.319 mmol, 64%), which was purified by semiprep HPLC (method F). HPLC (method A) 99%, t_R = 19.01 min. Mp 231−233 °C. ^{1}H NMR (400 MHz, DMSO-d_6) δ 10.11 (2H, s), 10.10 (2H, s), 9.17 (2H, s), 8.11 (2H, s), 7.96 (4H, d, J = 8.8 Hz), 7.62 (4H, d, J = 8.8 Hz), 7.42 (2H, d, J = 8.3 Hz), 7.35 (2H, d, J = 8.2 Hz), 7.25 (2H, t, J = 8.1 Hz), 2.76 (4H, t, J = 7.0 Hz), 2.50 (12H, m), 1.71 (8H, m) ppm. ^{13}C NMR (100 MHz, DMSO-d_6) δ 169.9, 164.8, 152.0, 142.5, 139.5, 139.3, 128.7, 128.5, 127.9, 117.2, 115.2, 114.3, 111.3, 53.3, 51.4, 35.8, 23.0 ppm. HRMS *m/z* calcd $C_{41}H_{46}N_8O_5$ $[M + H]^+$ 731.3664, found 731.3668.

1,3-Bis(4-(3-(4-(pyrrolidin-1-yl)butanamido)phenylcarbamoyl)phenyl)urea (10f). Following method 8, **7l** (150.0 mg, 0.500 mmol) was reacted with **3f** (494.2 mg, 1.998 mmol) to yield a white solid (173.4 mg, 0.228 mmol, 46%), which was purified by semiprep HPLC (method G). HPLC (method A) 97%, t_R = 20.40 min. Mp 249−252 °C. ^{1}H NMR (400 MHz, DMSO-d_6) δ 10.09 (2H, s), 9.91 (2H, s), 9.31 (2H, s), 8.11 (2H, s), 7.95 (4H, d, J = 8.5 Hz), 7.63 (4H, d, J = 8.5 Hz), 7.41 (2H, d, J = 8.1 Hz), 7.34 (2H, d, J = 7.9 Hz), 7.23 (2H, t, J = 8.0 Hz), 2.52 (12H, m), 2.37 (4H, t, J = 7.2 Hz), 1.78 (4H, m), 1.70 (8H, m) ppm. ^{13}C NMR (100 MHz, DMSO-d_6) δ 170.9, 164.7, 152.1, 142.6, 139.4, 139.4, 128.7, 128.4, 127.9, 117.2, 115.2, 114.3, 111.4, 54.9, 53.4, 34.1, 23.9, 22.9 ppm. HRMS *m/z* calcd $C_{43}H_{50}N_8O_5$ $[M + H]^+$ 759.3977, found 759.3975.

3-Amino-5-nitro-*N*-phenylbenzamide (11). 3-Amino-5-nitrobenzoic acid (1.00 g, 5.490 mmol) was dissolved in DMF (25 mL), and to this were added aniline (0.55 mL, 6.039 mmol, 1.1 equiv), HOBt (816.1 mg, 6.039 mmol, 1.1 equiv), and DCC (1.25 g, 6.039 mmol, 1.1 equiv), and the mixture was stirred under N_2 (g) at room temperature for 24 h. The precipitate was filtered from the reaction, the solvent was evaporated, and to the residue was added 5% NH_3 (aq) (100 mL). The product was extracted into EtOAc (3 × 100 mL), washed with brine (50 mL), and dried over $MgSO_4$. The desired product was purified by flash chromatography to yield an orange powder (1.29 g, 5.019 mmol, 91%). Mp 202−204 °C. ^{1}H NMR (400 MHz, DMSO-d_6) δ10.40 (1H, s), 7.90 (1H, t, J = 1.8 Hz), 7.77 (2H, d, J = 7.6 Hz), 7.57 (1H, t, J = 2.2 Hz), 7.51 (1H, t, J = 1.8 Hz), 7.37 (2H, t, J = 7.9 Hz), 7.12 (1H, t, J = 7.4 Hz), 6.09 (2H, s) ppm. ^{13}C NMR (100 MHz, DMSO-d_6) δ 164.2, 150.2, 148.7, 138.8, 136.9, 128.6, 123.9, 120.5, 118.8, 109.5, 108.6 ppm. HRMS *m/z* calcd $C_{13}H_{11}N_3O_3$ $[M + H]^+$ 258.0873, found 258.0867.

3-(2-Chloroacetamido)-5-nitro-*N*-phenylbenzamide (12a). Following method 1a, **11** (150.0 mg, 0.583 mmol) was reacted with 2-chloroacetyl chloride (0.10 mL, 1.255 mmol) to yield a pink solid (127.8 mg, 0.383 mmol, 66%). Mp 187 °C dec. ^{1}H NMR (400 MHz, DMSO-d_6) δ 11.03 (1H, s), 10.65 (1H, s), 8.82 (1H, t, J = 2.0 Hz), 8.59 (1H, t, J = 2.0 Hz), 8.46 (1H, t, J = 2.0 Hz), 7.78 (2H, dd, J = 8.6, 1.3 Hz), 7.40 (2H, m), 7.15 (1H, t, J = 7.3 Hz), 4.37 (2H, s) ppm. ^{13}C NMR (100 MHz, DMSO- d_6) δ 165.6, 163.1, 148.0, 139.7, 138.6, 136.8, 128.7, 124.6, 124.2, 120.6, 117.1, 116.0, 43.4 ppm. HRMS *m/z* calcd $C_{15}H_{12}ClN_3O_4$ $[M + H]^+$ 334.0589, found 334.0582.

3-(Acrylamido)-5-nitro-*N*-phenylbenzamide (12b). Following method 1a, **11** (1.50 g, 5.831 mmol) was reacted with 3-chloropropanoyl chloride (1.12 mL, 11.732 mmol) to yield a cream solid (1.22 g, 3.928 mmol, 67%). Mp 197−199 °C. ^{1}H NMR (400 MHz, DMSO-d_6) δ 10.67 (1H, s), 10.61 (1H, s), 8.93 (1H, t, J = 2.1 Hz), 8.55 (1H, t, J = 1.8 Hz), 8.51 (1H, t, J = 1.8 Hz), 7.76 (2H, dd, J = 8.6, 1.0 Hz), 7.39 (2H, m), 7.15 (1H, t, J = 7.4 Hz), 6.48 (1H, dd, J = 17.0, 9.9 Hz), 6.36 (1H, dd, J = 17.0, 2.0 Hz), 5.88 (1H, dd, J = 9.9, 2.0 Hz) ppm. ^{13}C NMR (100 MHz, DMSO-d_6) δ 163.8, 163.2, 147.9, 140.2, 138.5, 136.7, 131.0, 128.6, 128.4, 124.5, 124.1, 120.5, 116.6, 115.9 ppm. HRMS *m/z* calcd $C_{16}H_{13}N_3O_4$ $[M + H]^+$ 312.0976, found 312.0965.

3-(4-Chlorobutanamido)-5-nitro-*N*-phenylbenzamide (12c). Following method 1a, **11** (1.50 g, 5.831 mmol) was reacted with 4-chlorobutanoyl chloride (1.30 mL, 11.617 mmol) to yield a cream solid (1.94 g, 5.360 mmol, 92%). Mp 213−215 °C. ^{1}H NMR (400 MHz, DMSO-d_6) 10.69 (1H, s), 10.60 (1H, s), 8.85 (1H, t, J = 2.1 Hz), 8.52 (1H, t, J = 1.8 Hz), 8.44 (1H, t, J = 1.8 Hz), 7.78 (2H, dd, J = 8.6, 1.0 Hz), 7.39 (2H, m), 7.15 (1H, t, J = 7.4 Hz), 3.74 (2H, t, J = 6.5 Hz), 2.58 (2H, t, J = 7.3 Hz), 2.09 (2H, m) ppm. ^{13}C NMR (100 MHz, DMSO-d_6) 171.2, 163.3, 147.9, 140.4, 138.6, 136.7, 128.7, 124.3, 124.1, 120.6, 116.3, 115.7, 44.9, 33.4, 27.6 ppm. HRMS *m/z* calcd $C_{17}H_{16}ClN_3O_4$ $[M + H]^+$ 362.0908, found 362.0900.

3-(2-(Pyrrolidin-1-yl)acetamido)-5-nitro-*N*-phenylbenzamide (13a). Following method 2a, **12a** (102.2 mg, 0.306 mmol) was reacted with pyrrolidine (0.05 mL, 5.990 mmol) to yield a beige solid (102.9 mg, 0.279 mmol, 91%). Mp 181−184 °C. ^{1}H NMR (400 MHz, DMSO-d_6) δ 10.57 (1H, s), 10.41 (1H, s), 8.92 (1H, t, J = 2.0 Hz), 8.58 (1H, t, J = 1.7 Hz), 8.51 (1H, t, J = 1.8 Hz), 7.77 (2H, m), 7.39 (2H, m), 7.15 (1H, t, J = 7.3 Hz), 3.33 (2H, s), 2.57 (4H, m), 1.72 (4H, m) ppm. ^{13}C NMR (100 MHz, DMSO-d_6) δ 170.0, 163.4, 147.9, 140.1, 138.7, 136.7, 128.7, 124.9, 124.1, 120.6, 116.5, 116.2, 59.5, 53.7, 23.5 ppm. HRMS *m/z* calcd $C_{19}H_{20}N_4O_4$ $[M + H]^+$ 369.1557, found 369.1539.

3-(3-(Pyrrolidin-1-yl)propanamido)-5-nitro-*N*-phenylbenzamide (13b). Following method 2a, **12b** (1.00 g, 3.212 mmol) was reacted with pyrrolidine (0.54 mL, 6.469 mmol) to yield a cream solid (947.8 mg, 2.478 mmol, 77%). Mp 151−153 °C. ^{1}H NMR (400 MHz, DMSO-d_6) δ 10.69 (1H, s), 10.59 (1H, s), 8.85 (1H, t, J = 1.8 Hz), 8.51 (1H, s), 8.41 (1H, s), 7.77 (2H, d, J = 8.0 Hz), 7.38 (2H, t, J = 7.8 Hz), 7.14 (1H, t, J = 7.4 Hz), 2.75 (2H, t, J = 6.9 Hz), 2.55 (2H, t, J = 6.9 Hz), 2.48 (4H, m), 1.68 (4H, m) ppm. ^{13}C NMR (100 MHz, DMSO- d_6) δ 171.0, 163.2, 147.8, 140.4, 138.6, 136.6, 128.6, 124.1, 124.0, 120.5, 116.1, 115.5, 53.3, 51.2, 36.0, 23.0 ppm. HRMS *m/z* calcd $C_{20}H_{22}N_4O_4$ $[M + H]^+$ 383.1714, found 383.1727.

3-(4-(Pyrrolidin-1-yl)butanamido)-5-nitro-*N*-phenylbenzamide (13c). Following method 2b, **12c** (1.00 g, 2.764 mmol) was reacted with pyrrolidine (0.69 mL, 8.266 mmol) to yield a pale-yellow solid (861.1 mg, 2.172 mmol, 79%). Mp 157−161 °C. ^{1}H NMR (400 MHz, DMSO-d_6) δ 10.58 (2H, s), 8.84 (1H, t, J = 2.0 Hz), 8.50 (1H, t, J = 1.8 Hz), 8.42 (1H, t, J = 1.7 Hz), 7.77 (2H, d, J = 8.6 Hz), 7.38 (2H, m), 7.14 (1H, t, J = 7.7 Hz), 2.43 (8H, m), 1.79 (2H, m), 1.66 (4H, m) ppm. ^{13}C NMR (100 MHz, DMSO-d_6) δ 172.1, 163.2, 147.8, 140.5, 138.5, 136.6, 128.6, 124.1, 124.0, 120.5, 116.0, 115.5, 54.9, 53.4, 34.4, 24.0, 23.0 ppm. HRMS *m/z* calcd $C_{21}H_{24}N_4O_4$ $[M + H]^+$ 397.1876, found 397.1860.

3-(2-(Pyrrolidin-1-yl)acetamido)-5-amino-*N*-phenylbenzamide (14a). Following method 3b, **13a** (300.0 mg, 0.814 mmol) was reduced to yield a brown solid (254.1 mg, 0.751 mmol, 92%). Mp 88−91 °C. ^{1}H NMR (400 MHz, DMSO-d_6) δ10.16 (1H, s), 9.61

(1H, s), 7.80 (2H, d, $J = 7.7$ Hz), 7.39 (2H, t, $J = 7.8$ Hz), 7.29 (1H, s), 7.20 (1H, s), 7.13 (1H, t, $J = 7.4$ Hz), 6.82 (1H, s), 5.43 (2H, s), 3.28 (2H, s) 2.65 (4H, m), 1.81 (4H, m) ppm. ^{13}C NMR (100 MHz, DMSO-d_6) δ 168.6, 166.4, 149.0, 139.4, 139.1, 136.5, 128.5, 123.3, 120.1, 108.4, 107.5, 106.7, 59.4, 53.7, 23.5 ppm. HRMS *m/z* calcd $C_{19}H_{22}N_4O_2$ $[M + H]^+$ 339.1815, found 339.1797.

3-(3-(Pyrrolidin-1-yl)propanamido)-5-amino-*N*-phenylbenzamide (14b). Following method 3b, **13b** (300.0 mg, 0.784 mmol) was reduced to yield a white solid (225.7 mg, 0.640 mmol, 82%). Mp 196−198 °C. ^{1}H NMR (400 MHz, DMSO-d_6) δ 10.12 (1H, s), 9.97 (1H, s), 7.74 (2H, d, $J = 7.7$ Hz), 7.32 (2H, t, $J = 7.9$ Hz), 7.16 (1H, s), 7.10 (1H, s), 7.06 (1H, t, $J = 7.4$ Hz), 6.72 (1H, s), 5.35 (2H, s), 2.64 (2H, t, $J = 7.0$ Hz), 2.45 (6H, m), 1.68 (4H, m) ppm. ^{13}C NMR (100 MHz, DMSO-d_6) δ 170.0, 166.5, 148.9, 139.7, 139.3, 136.5, 128.4, 123.2, 119.9, 107.9, 107.1, 106.4, 53.3, 51.5, 36.0, 23.1 ppm. HRMS *m/z* calcd $C_{20}H_{24}N_4O_2$ $[M + H]^+$ 353.1972, found 353.1955.

3-(4-(Pyrrolidin-1-yl)butanamido)-5-amino-*N*-phenylbenzamide (14c). Following method 3b, **13c** (801.0 mg, 2.021 mmol) was reduced to yield a white solid (646.9 mg, 1.765 mmol, 87%). Mp 159−161 °C. ^{1}H NMR (400 MHz, DMSO-d_6) δ 10.07 (1H, s), 9.75 (1H, s), 7.74 (2H, d, $J = 8.4$ Hz), 7.32 (2H, t, $J = 8.0$ Hz), 7.16 (1H, t, $J = 1.8$ Hz), 7.12 (1H, t, $J = 1.6$ Hz), 7.06 (1H, t, $J = 7.4$ Hz), 6.72 (1H, t, $J = 1.7$ Hz), 5.30 (2H, s), 2.42 (4H, m), 2.40 (2H, t, $J = 7.2$ Hz), 2.30 (2H, t, $J = 7.4$ Hz), 1.74 (2H, m), 1.67 (4H, m) ppm. ^{13}C NMR (100 MHz, DMSO-d_6) δ 171.0, 166.6, 148.8, 139.8, 139.3, 136.5, 128.4, 123.2, 119.9, 107.9, 107.2, 106.4, 55.0, 53.4, 34.4, 24.3, 23.0 ppm. HRMS *m/z* calcd $C_{21}H_{26}N_4O_2$ $[M + H]^+$ 367.2134, found 367.2088.

1,3-Bis(3-(phenylcarbamoyl)-5-(2-(pyrrolidin-1-yl)acetamido)phenyl)urea (15a). Following method 6b, **14a** (500.0 mg, 1.478 mmol) was reacted with CDI (239.7 mg, 1.478 mmol) to yield a white solid (231.0 mg, 0.329 mmol, 44%), which was purified by semiprep HPLC (method F). HPLC (method A) 96%, $t_R = 21.02$ min. Mp 179−181 °C. ^{1}H NMR (400 MHz, DMSO-d_6) δ 10.28 (2H, s), 9.92 (2H, s), 8.94 (2H, s), 8.14 (2H, t, $J = 1.7$ Hz), 7.77 (4H, d, $J = 7.8$ Hz), 7.72 (2H, t, $J = 1.7$ Hz), 7.70 (2H, t, $J = 1.7$ Hz), 7.36 (4H, t, $J = 7.9$ Hz), 7.11 (2H, t, $J = 7.4$ Hz), 3.33 (4H, s), 2.66 (8H, m), 1.78 (8H, m) ppm. ^{13}C NMR (100 MHz, DMSO-d_6) δ 168.7, 165.7, 152.2, 139.8, 139.1, 139.0, 136.4, 128.5, 123.5, 120.1, 112.5, 112.5, 111.9, 59.2, 53.6, 23.4 ppm. HRMS *m/z* calcd $C_{39}H_{42}N_8O_5$ $[M + H]^+$ 703.3351, found 703.3369.

1,3-Bis(3-(phenylcarbamoyl)-5-(3-(pyrrolidin-1-yl)propanamido)phenyl)urea (15b). Following method 6b, **14b** (500.0 mg, 1.419 mmol) was reacted with CDI (230.1 mg, 1.419 mmol) to yield a white solid (245.8 mg, 0.336 mmol, 47%), which was purified by semiprep HPLC (method F). HPLC (method A) 99%, $t_R = 21.01$ min. Mp 167−169 °C. ^{1}H NMR (400 MHz, DMSO-d_6) δ 10.27 (2H, s), 10.22 (2H, s), 8.90 (2H, s), 8.08 (2H, s), 7.74 (4H, d, $J = 8.6$ Hz), 7.65 (2H, s), 7.62 (2H, s), 7.33 (4H, t, $J = 7.8$ Hz), 7.07 (2H, t, $J = 7.4$ Hz), 2.75 (4H, t, $J = 6.9$ Hz), 2.50 (12H, m), 1.68 (8H, m) ppm. ^{13}C NMR (100 MHz, DMSO-d_6) δ 170.2, 165.8, 152.2, 139.8, 139.6, 139.1, 136.5, 128.5, 123.4, 120.1, 112.1, 112.1, 111.4, 53.3, 51.3, 35.8, 23.0 ppm. HRMS *m/z* calcd $C_{41}H_{46}N_8O_5$ $[M + H]^+$ 731.3664, found 731.3674.

1,3-Bis(3-(phenylcarbamoyl)-5-(4-(pyrrolidin-1-yl)butanamido)phenyl)urea (15c). Following method 6b, **14c** (500.0 mg, 1.364 mmol) was reacted with CDI (221.2 mg, 1.364 mmol) to yield a white solid (288.9 mg, 0.381 mmol, 56%), which was purified by semiprep HPLC (method F). HPLC (method A) 97%, $t_R = 21.89$ min. Mp 176−178 °C. ^{1}H NMR (400 MHz, DMSO-d_6) δ 10.28 (2H, s), 10.09 (2H, s), 8.91 (2H, s), 8.10 (2H, s), 7.76 (4H, d, $J = 7.7$ Hz), 7.69 (2H, s), 7.65 (2H, s), 7.36 (4H, t, $J = 7.4$ Hz), 7.10 (2H, t, $J = 7.4$ Hz), 2.46 (12H, m), 2.39 (4H, t, $J = 7.4$ Hz), 1.78 (4H, m), 1.69 (8H, m) ppm. ^{13}C NMR (100 MHz, DMSO-d_6) δ 171.3, 165.9, 152.2, 139.7, 139.7, 139.1, 136.4, 128.5, 123.4, 120.1, 112.1, 112.0, 111.5, 55.0, 53.4, 34.3, 24.1, 23.0 ppm. HRMS *m/z* calcd $C_{43}H_{50}N_8O_5$ $[M + H]^+$ 759.3977, found 759.4016.

Acknowledgment. We are grateful to CRUK (Program Grant No. C129/A4489) and the EU (FP6 Molecular Cancer Medicine) for support (S.N.) and to NIH for Grant GM61587 (W.D.W.). We are also grateful to various colleagues for useful advice and discussions.

Supporting Information Available: Experimental procedures and characterization of side chain building blocks, quinazoline dione ligands; HPLC purity analysis results; FRET-based correlations; TRAP-LIG data for **9a**−**c**; MCF7 population growth; senescence and telomere end−end fusion data; additional modeled ligand−DNA complexes. This material is available free of charge via the Internet at http://pubs.acs.org.

References

(1) Burge, S.; Parkinson, G. N.; Hazel, P.; Todd, A. K.; Neidle, S. Quadruplex DNA: sequence, topology and structure. *Nucleic Acids Res.* **2006**, *34*, 5402–5415.
(2) Gellert, M.; Lipsett, M. N.; Davies, D. R. Helix formation by guanylic acid. *Proc. Natl. Acad. Sci U.S.A.* **1962**, *48*, 2013–2018.
(3) Patel, D. J.; Phan, A. T.; Kuryavyi, V. Human telomere, oncogenic promoter and 5′-UTR G-quadruplexes: diverse higher order DNA and RNA targets for cancer therapeutics. *Nucleic Acids Res.* **2007**, *35*, 7429–7455.
(4) Zimmerman, S. B.; Cohen, G. H.; Davies, D. R. X-ray fiber diffraction and model-building study of polyguanylic acid and polyinosinic acid. *J. Mol. Biol.* **1975**, *92*, 181–192.
(5) Meyne, J.; Ratliff, R. L.; Moyzis, R. K. Conservation of the human telomere sequence (TTAGGG)n among vertebrates. *Proc. Natl. Acad. Sci U.S.A.* **1989**, *86*, 7049–7053.
(6) Moyzis, R. K.; Buckingham, J. M.; Cram, L. S.; Dani, M.; Deaven, L. L.; Jones, M. D.; Meyne, J.; Ratliff, R. L.; Wu, J. R. A highly conserved repetitive DNA sequence, (TTAGGG)n, present at the telomeres of human chromosomes. *Proc. Natl. Acad. Sci U.S.A.* **1988**, *85*, 6622–6626.
(7) Makarov, V. L.; Hirose, Y.; Langmore, J. P. Long G tails at both ends of human chromosomes suggest a C strand degradation mechanism for telomere shortening. *Cell* **1997**, *88*, 657–666.
(8) Sfeir, A. J.; Chai, W.; Shay, J. W.; Wright, W. E. Telomere-end processing the terminal nucleotides of human chromosomes. *Mol. Cell* **2005**, *18*, 131–138.
(9) Lei, M.; Podell, E. R.; Cech, T. R. Structure of human POT1 bound to telomeric single-stranded DNA provides a model for chromosome end-protection. *Nat. Struct. Mol. Biol.* **2004**, *11*, 1223–1229.
(10) de Lange., T. Shelterin: the protein complex that shapes and safeguards human telomeres. *Genes Dev.* **2005**, *19*, 2100–2110.
(11) Loayza, D.; de Lange, T. POT1 as a terminal transducer of TRF1 telomere length control. *Nature* **2003**, *423*, 1013–1018.
(12) Loayza, D.; Parsons, H.; Donigian, J.; Hoke, K.; de Lange, T. DNA binding features of human POT1: a nonamer 5′-TAGGGTTAG-3′ minimal binding site, sequence specificity, and internal binding to multimeric sites. *J. Biol. Chem.* **2004**, *279*, 13241–13248.
(13) Harley, C. B.; Futcher, A. B.; Greider, C. W. Telomeres shorten during ageing of human fibroblasts. *Nature* **1990**, *345*, 458–460.
(14) Morin, G. B. The human telomere terminal transferase enzyme is a ribonucleoprotein that synthesizes TTAGGG repeats. *Cell* **1989**, *59*, 521–529.
(15) Hanahan, D.; Weinberg, R. A. The hallmarks of cancer. *Cell* **2000**, *100*, 57–70.
(16) Kim, N. W.; Piatyszek, M. A.; Prowse, K. R.; Harley, C. B.; West, M. D.; Ho, P. L.; Coviello, G. M.; Wright, W. E.; Weinrich, S. L.; Shay, J. W. Specific association of human telomerase activity with immortal cells and cancer. *Science* **1994**, *266*, 2011–2015.
(17) Greider, C. W.; Blackburn, E. H. Identification of a specific telomere terminal transferase activity in tetrahymena extracts. *Cell* **1985**, *43*, 405–413.
(18) Shay, J. W.; Bacchetti, S. A survey of telomerase activity in human cancer. *Eur. J. Cancer* **1997**, *33*, 787–791.
(19) Cuenca, F.; Greciano, O.; Gunaratnam, M.; Haider, S.; Munnur, D.; Nanjunda, R.; Wilson, W. D.; Neidle, S. Tri- and tetra-substituted naphthalene diimides as potent G-quadruplex ligands. *Bioorg. Med. Chem. Lett.* **2008**, *18*, 1668–1673.
(20) Kim, M. Y.; Vankayalapati, H.; Shin-Ya, K.; Wierzba, K.; Hurley, L. H. Telomestatin, a potent telomerase inhibitor that interacts quite specifically with the human telomeric intramolecular G-quadruplex. *J. Am. Chem. Soc.* **2002**, *124*, 2098–2099.
(21) Gowan, S. M.; Harrison, J. R.; Patterson, L.; Valenti, M.; Read, M. A.; Neidle, S.; Kelland, L. R. A G-quadruplex-interactive potent small-molecule inhibitor of telomerase exhibiting in vitro and in vivo antitumor activity. *Mol. Pharmacol.* **2002**, *61*, 1154–1162.
(22) Gunaratnam, M.; Greciano, O.; Martins, C.; Reszka, A. P.; Schultes, C. M.; Morjani, H.; Riou, J. F.; Neidle, S. Mechanism of acridine-

based telomerase inhibition and telomere shortening. *Biochem. Pharmacol.* **2007**, *74*, 679–689.
(23) Harrison, R. J.; Gowan, S. M.; Kelland, L. R.; Neidle, S. Human telomerase inhibition by substituted acridine derivatives. *Bioorg. Med. Chem. Lett.* **1999**, *9*, 2463–2468.
(24) Harrison, R. J.; Cuesta, J.; Chessari, G.; Read, M. A.; Basra, S. K.; Reszka, A. P.; Morrell, J.; Gowan, S. M.; Incles, C. M.; Tanious, F. A.; Wilson, W. D.; Kelland, L. R.; Neidle, S. Trisubstituted acridine derivatives as potent and selective telomerase inhibitors. *J. Med. Chem.* **2003**, *46*, 4463–4476.
(25) Harrison, R. J.; Reszka, A. P.; Haider, S. M.; Romagnoli, B.; Morrell, J.; Read, M. A.; Gowan, S. M.; Incles, C. M.; Kelland, L. R.; Neidle, S. Evaluation of by disubstituted acridone derivatives as telomerase inhibitors: the importance of G-quadruplex binding. *Bioorg. Med. Chem. Lett.* **2004**, *14*, 5845–5849.
(26) Heald, R. A.; Modi, C.; Cookson, J. C.; Hutchinson, I.; Laughton, C. A.; Gowan, S. M.; Kelland, L. R.; Stevens, M. F. Antitumor polycyclic acridines. 8. Synthesis and telomerase-inhibitory activity of methylated pentacyclic acridinium salts. *J. Med. Chem.* **2002**, *45*, 590–597.
(27) Leonetti, C.; Amodei, S.; D'Angelo, C.; Rizzo, A.; Benassi, B.; Antonelli, A.; Elli, R.; Stevens, M. F.; D'Incalci, M.; Zupi, G.; Biroccio, A. Biological activity of the G-quadruplex ligand RHPS4 (3,11-difluoro-6,8,13-trimethyl-8*H*-quino[4,3,2-*kl*]acridinium methosulfate) is associated with telomere capping alteration. *Mol. Pharmacol.* **2004**, *66*, 1138–1146.
(28) Martins, C.; Gunaratnam, M.; Stuart, J.; Makwana, V.; Greciano, O.; Reszka, A. P.; Kelland, L. R.; Neidle, S. Structure-based design of benzylamino-acridine compounds as G-quadruplex DNA telomere targeting agents. *Bioorg. Med. Chem. Lett.* **2007**, *17*, 2293–2298.
(29) Mergny, J. L.; Lacroix, L.; Teulade-Fichou, M. P.; Hounsou, C.; Guittat, L.; Hoarau, M.; Arimondo, P. B.; Vigneron, J. P.; Lehn, J. M.; Riou, J. F.; Garestier, T.; Helene, C. Telomerase inhibitors based on quadruplex ligands selected by a fluorescence assay. *Proc. Natl. Acad. Sci. U.S.A.* **2001**, *98*, 3062–3067.
(30) Moore, M. J.; Schultes, C. M.; Cuesta, J.; Cuenca, F.; Gunaratnam, M.; Tanious, F. A.; Wilson, W. D.; Neidle, S. Trisubstituted acridines as G-quadruplex telomere targeting agents. Effects of extensions of the 3,6- and 9-side chains on quadruplex binding, telomerase activity, and cell proliferation. *J. Med. Chem.* **2006**, *49*, 582–599.
(31) Moorhouse, A. D.; Santos, A. M.; Gunaratnam, M.; Moore, M.; Neidle, S.; Moses, J. E. Stabilization of G-quadruplex DNA by highly selective ligands via click chemistry. *J. Am. Chem. Soc.* **2006**, *128*, 15972–15973.
(32) Read, M.; Harrison, R. J.; Romagnoli, B.; Tanious, F. A.; Gowan, S. H.; Reszka, A. P.; Wilson, W. D.; Kelland, L. R.; Neidle, S. Structure-based design of selective and potent G quadruplex-mediated telomerase inhibitors. *Proc. Natl. Acad. Sci U.S.A.* **2001**, *98*, 4844–4849.
(33) Read, M. A.; Wood, A. A.; Harrison, J. R.; Gowan, S. M.; Kelland, L. R.; Dosanjh, H. S.; Neidle, S. Molecular modeling studies on G-quadruplex complexes of telomerase inhibitors: structure−activity relationships. *J. Med. Chem.* **1999**, *42*, 4538–4546.
(34) Schultes, C. M.; Guyen, B.; Cuesta, J.; Neidle, S. Synthesis, biophysical and biological evaluation of 3,6-bis-amidoacridines with extended 9-anilino substituents as potent G-quadruplex-binding telomerase inhibitors. *Bioorg. Med. Chem. Lett.* **2004**, *14*, 4347–4351.
(35) Sun, D.; Thompson, B.; Cathers, B. E.; Salazar, M.; Kerwin, S. M.; Trent, J. O.; Jenkins, T. C.; Neidle, S.; Hurley, L. H. Inhibition of human telomerase by a G-quadruplex-interactive compound. *J. Med. Chem.* **1997**, *40*, 2113–2116.
(36) Wheelhouse, R. T.; Sun, D. K.; Han, H. Y.; Han, F. X. G.; Hurley, L. H. Cationic porphyrins as telomerase inhibitors: the interaction of tetra-(*N*-methyl-4-pyridyl)porphine with quadruplex DNA. *J. Am. Chem. Soc.* **1998**, *120*, 3261–3262.
(37) Huppert, J. L.; Balasubramanian, S. G-quadruplexes in promoters throughout the human genome. *Nucleic Acids Res.* **2007**, *35*, 406–413.
(38) Phan, A. T.; Modi, Y. S.; Patel, D. J. Propeller-type parallel-stranded G-quadruplexes in the human c-myc promoter. *J. Am. Chem. Soc.* **2004**, *126*, 8710–8716.
(39) Phan, A. T.; Kuryavyi, V.; Gaw, H. Y.; Patel, D. J. Small-molecule interaction with a five-guanine-tract G-quadruplex structure from the human MYC promoter. *Nat. Chem. Biol.* **2005**, *1*, 167–173.
(40) Siddiqui-Jain, A.; Grand, C. L.; Bearss, D. J.; Hurley, L. H. Direct evidence for a G-quadruplex in a promoter region and its targeting with a small molecule to repress c-MYC transcription. *Proc. Natl. Acad. Sci. U.S.A.* **2002**, *99*, 11593–11598.
(41) Simonsson, T.; Pecinka, P.; Kubista, M. DNA tetraplex formation in the control region of c-myc. *Nucleic Acids Res.* **1998**, *26*, 1167–1172.
(42) Fernando, H.; Reszka, A. P.; Huppert, J.; Ladame, S.; Rankin, S.; Venkitaraman, A. R.; Neidle, S.; Balasubramanian, S. A conserved quadruplex motif located in a transcription activation site of the human c-kit oncogene. *Biochemistry* **2006**, *45*, 7854–7860.
(43) Phan, A. T.; Kuryavyi, V.; Burge, S.; Neidle, S.; Patel, D. J. Structure of an unprecedented G-quadruplex scaffold in the human c-kit promoter. *J. Am. Chem. Soc.* **2007**, *129*, 4386–4392.
(44) Rankin, S.; Reszka, A. P.; Huppert, J.; Zloh, M.; Parkinson, G. N.; Todd, A. K.; Ladame, S.; Balasubramanian, S.; Neidle, S. Putative DNA quadruplex formation within the human c-kit oncogene. *J. Am. Chem. Soc.* **2005**, *127*, 10584–10589.
(45) Dexheimer, T. S.; Sun, D.; Hurley, L. H. Deconvoluting the structural and drug-recognition complexity of the G-quadruplex-forming region upstream of the bcl-2 P1 promoter. *J. Am. Chem. Soc.* **2006**, *128*, 5404–5415.
(46) Cogoi, S.; Xodo, L. E. G-quadruplex formation within the promoter of the KRAS proto-oncogene and its effect on transcription. *Nucleic Acids Res.* **2006**, *34*, 2536–2549.
(47) Kumari, S.; Bugaut, A.; Huppert, J. L.; Balasubramanian, S. An RNA G-quadruplex in the 5′ UTR of the NRAS proto-oncogene modulates translation. *Nat. Chem. Biol.* **2007**, *3*, 218–221.
(48) Soldatenkov, V. A.; Vetcher, A. A.; Duka, T.; Ladame, S. First evidence of a functional interaction between DNA quadruplexes and poly(ADP-ribose) polymerase-1. *ACS Chem. Biol.* **2008**, *3*, 214–219.
(49) Blackburn, E. H. Telomere states and cell fates. *Nature* **2000**, *408*, 53–56.
(50) Blackburn, E. H. Switching and signaling at the telomere. *Cell* **2001**, *106*, 661–673.
(51) Smogorzewska, A.; de Lange, T. Regulation of telomerase by telomeric proteins. *Annu. Rev. Biochem.* **2004**, *73*, 177–208.
(52) Li, G. Z.; Eller, M. S.; Hanna, K.; Gilchrest, B. A. Signaling pathway requirements for induction of senescence by telomere homolog oligonucleotides. *Exp. Cell Res.* **2004**, *301*, 189–200.
(53) Herbig, U.; Jobling, W. A.; Chen, B. P.; Chen, D. J.; Sedivy, J. M. Telomere shortening triggers senescence of human cells through a pathway involving ATM, p53, and p21(CIP1), but not p16(INK4a). *Mol. Cell* **2004**, *14*, 501–513.
(54) Murnane, J. P. Telomeres and chromosome instability. *DNA Repair* **2006**, *5*, 1082–1092.
(55) Gilley, D.; Tanaka, H.; Herbert, B. S. Telomere dysfunction in aging and cancer. *Int. J. Biochem. Cell Biol.* **2005**, *37*, 1000–1013.
(56) Shin-Ya, K.; Wierzba, K.; Matsuo, K.; Ohtani, T.; Yamada, Y.; Furihata, K.; Hayakawa, Y.; Seto, H. Telomestatin, a novel telomerase inhibitor from *Streptomyces anulatus*. *J. Am. Chem. Soc.* **2001**, *123*, 1262–1263.
(57) Hahn, W. C.; Stewart, S. A.; Brooks, M. W.; York, S. G.; Eaton, E.; Kurachi, A.; Beijersbergen, R. L.; Knoll, J. H.; Meyerson, M.; Weinberg, R. A. Inhibition of telomerase limits the growth of human cancer cells. *Nat. Med.* **1999**, *5*, 1164–1170.
(58) Harley, C. B. Telomerase and cancer therapeutics. *Nat. Rev. Cancer* **2008**, *8*, 167–179.
(59) Herbert, B. S.; Gellert, G. C.; Hochreiter, A.; Pongracz, K.; Wright, W. E.; Zielinska, D.; Chin, A. C.; Harley, C. B.; Shay, J. W.; Gryaznov, S. M. Lipid modification of GRN163, an N3′→P5′ thiophosphoramidate oligonucleotide, enhances the potency of telomerase inhibition. *Oncogene* **2005**, *24*, 5262–5268.
(60) Kelland, L. Targeting the limitless replicative potential of cancer: the telomerase/telomere pathway. *Clin. Cancer Res.* **2007**, *13*, 4960–4963.
(61) Burger, A. M.; Dai, F.; Schultes, C. M.; Reszka, A. P.; Moore, M. J.; Double, J. A.; Neidle, S. The G-quadruplex-interactive molecule BRACO-19 inhibits tumor growth, consistent with telomere targeting and interference with telomerase function. *Cancer Res.* **2005**, *65*, 1489–1496.
(62) Gomez, D.; O'Donohue, M. F.; Wenner, T.; Douarre, C.; Macadre, J.; Koebel, P.; Giraud-Panis, M. J.; Kaplan, H.; Kolkes, A.; Shin-Ya, K.; Riou, J. F. The G-quadruplex ligand telomestatin inhibits POT1 binding to telomeric sequences in vitro and induces GFP-POT1 dissociation from telomeres in human cells. *Cancer Res.* **2006**, *66*, 6908–6912.
(63) Gomez, D.; Wenner, T.; Brassart, B.; Douarre, C.; O'Donohue, M. F.; El, K. V.; Shin-Ya, K.; Morjani, H.; Trentesaux, C.; Riou, J. F. Telomestatin-induced telomere uncapping is modulated by POT1 through G-overhang extension in HT1080 human tumor cells. *J. Biol. Chem.* **2006**, *281*, 38721–38729.
(64) Incles, C. M.; Schultes, C. M.; Kempski, H.; Koehler, H.; Kelland, L. R.; Neidle, S. A G-quadruplex telomere targeting agent produces p16-associated senescence and chromosomal fusions in human prostate cancer cells. *Mol. Cancer Ther.* **2004**, *3*, 1201–1206.
(65) Phatak, P.; Cookson, J. C.; Dai, F.; Smith, V.; Gartenhaus, R. B.; Stevens, M. F.; Burger, A. M. Telomere uncapping by the G-quadruplex ligand RHPS4 inhibits clonogenic tumour cell growth in vitro and in vivo consistent with a cancer stem cell targeting mechanism. *Br. J. Cancer* **2007**, *96*, 1223–1233.
(66) Salvati, E.; Leonetti, C.; Rizzo, A.; Scarsella, M.; Mottolese, M.; Galati, R.; Sperduti, I.; Stevens, M. F.; D'Incalci, M.; Blasco, M.; Chiorino, G.; Bauwens, S.; Horard, B.; Gilson, E.; Stoppacciaro, A.; Zupi, G.; Biroccio, A. Telomere damage induced by the G-quadruplex

ligand RHPS4 has an antitumor effect. *J. Clin. Invest.* **2007**, *117*, 3236–3247.
(67) Tahara, H.; Shin-Ya, K.; Seimiya, H.; Yamada, H.; Tsuruo, T.; Ide, T. G-Quadruplex stabilization by telomestatin induces TRF2 protein dissociation from telomeres and anaphase bridge formation accompanied by loss of the 3′ telomeric overhang in cancer cells. *Oncogene* **2006**, *25*, 1955–1966.
(68) Parkinson, G. N.; Lee, M. P.; Neidle, S. Crystal structure of parallel quadruplexes from human telomeric DNA. *Nature* **2002**, *417*, 876–880.
(69) Phan, A. T.; Patel, D. J. Two-repeat human telomeric d(TAGGGTTAGGGT) sequence forms interconverting parallel and antiparallel G-quadruplexes in solution: distinct topologies, thermodynamic properties, and folding/unfolding kinetics. *J. Am. Chem. Soc.* **2003**, *125*, 15021–15027.
(70) Phan, A. T.; Luu, K. N.; Patel, D. J. Different loop arrangements of intramolecular human telomeric (3 + 1) G-quadruplexes in K+ solution. *Nucleic Acids Res.* **2006**, *34*, 5715–5719.
(71) Phan, A. T.; Kuryavyi, V.; Luu, K. N.; Patel, D. J. Structure of two intramolecular G-quadruplexes formed by natural human telomere sequences in K+ solution. *Nucleic Acids Res.* **2007**, *35*, 6517–6525.
(72) Wang, Y.; Patel, D. J. Solution structure of the human telomeric repeat $d[AG_3(T_2AG_3)_3]$ G-tetraplex. *Structure* **1993**, *1*, 263–282.
(73) Gavathiotis, E.; Heald, R. A.; Stevens, M. F.; Searle, M. S. Drug recognition and stabilisation of the parallel-stranded DNA quadruplex $d(TTAGGGT)_4$ containing the human telomeric repeat. *J. Mol. Biol.* **2003**, *334*, 25–36.
(74) Haider, S. M.; Parkinson, G. N.; Neidle, S. Structure of a G-quadruplex-ligand complex. *J. Mol. Biol.* **2003**, *326*, 117–125.
(75) Parkinson, G. N.; Ghosh, R.; Neidle, S. Structural basis for binding of porphyrin to human telomeres. *Biochemistry* **2007**, *46*, 2390–2397.
(76) Campbell, N. H.; Parkinson, G. N.; Reszka, A. P.; Neidle, S. Structural basis of DNA quadruplex recognition by an acridine drug. *J. Am. Chem. Soc.* **2008**, *130*, 6722–6724.
(77) Dugave, C. *Cis*−*Trans Isomerization in Biochemistry*; Wiley-VCH: Weinheim, Germany, 2006.
(78) Rajnikant; Dinesh; Deshmukh, M. B.; Kamni. Synthesis, X-ray strucutre and N−H···O interactions in 1,3-diphenyl urea. *Bull. Mater. Sci.* **2006**, *29*, 239–242.
(79) Monchaud, D.; Teulade-Fichou, M. P. A hitchhiker's guide to G-quadruplex ligands. *Org. Biomol. Chem.* **2008**, *6*, 627–636.
(80) Paul, R.; Anderson, G. W. *N,N′*-Carbonyldiimidazole, a new peptide forming reagent. *J. Am. Chem. Soc.* **1960**, *82*, 4596–4600.
(81) Smirnova, J.; Wöll, D.; Pfleiderer, W.; Steiner, U. E. Synthesis of caged nucleosides with photoremovable protecting groups linked to intramolecular antennae. *Helv. Chim. Acta* **2005**, *88*, 891–904.
(82) Batey, R. A.; Shen, M.; Santhakumar, V.; Yoshina-Ishii, C. Parallel synthesis of tri- and tetrasubstituted ureas from carbamoyl imidazolium salts. *Comb. Chem. High Throughput Screening* **2002**, *5*, 219–232.
(83) Coyne, W. C.; Cusic, J. W. 3,4-Dihydro-2(1*H*)-quinazolinones. *J. Med. Chem.* **1968**, *11*, 1208–1213.
(84) Curran, D. P.; Kuo, L. H. Altering the stereochemistry of allylation reactions of cyclic α-sulfinyl radicals with diarylureas. *J. Org. Chem.* **1994**, *59*, 3259–3261.
(85) Wuts, P. G. M.; Greene, T. W. *Greene's Protective Groups in Organic Synthesis*; Wiley & Sons Inc.: Hoboken, NJ, 2007.
(86) You, S.-L.; Kelly, J. W. Total stnthesis of didomolamides A and B. *Tetrahedron Lett.* **2005**, *46*, 2567–2570.
(87) Mas, T.; Pardo, C.; Salort, F.; Elguero, J.; Torres, M. R. A new entry to bis-Tröger's bases. *Eur. J. Org. Chem.* **2004**, 1104.
(88) Mergny, J. L.; Maurizot, J. C. Fluorescence resonance energy transfer as a probe for G-quartet formation by a telomeric repeat. *ChemBioChem* **2001**, *2*, 124–132.
(89) De Cian, A.; Guittat, L.; Shin-Ya, K.; Riou, J. F.; Mergny, J. L. Affinity and selectivity of G4 ligands measured by FRET. *Nucleic Acids Symp. Ser.* **2005**, 235–236.
(90) Nguyen, B.; Tanious, F. A.; Wilson, W. D. Biosensor-surface plasmon resonance: quantitative analysis of small molecule-nucleic acid interactions. *Methods* **2007**, *42*, 150–161.
(91) White, E. W.; Tanious, F.; Ismail, M. A.; Reszka, A. P.; Neidle, S.; Boykin, D. W.; Wilson, W. D. Structure-specific recognition of quadruplex DNA by organic cations: influence of shape, substituents and charge. *Biophys. Chem.* **2007**, *126*, 140–153.
(92) *Insight II: Modeling Environment*; Molecular Simulations Inc.: San Diego, CA, 2000.
(93) Duber-Osguthorpe, P.; Roberts, V. A.; Osguthorpe, D. J.; Wolff, J.; Genest, M.; Hagler, A. T. Structure and energetics of ligand binding to proteins: *Escherichia coli* dihydrofolate reductase-trimethoprim, a drug-receptor system. *Proteins* **1988**, *4*, 31–47.
(94) Franceschin, M.; Alvino, A.; Casagrande, V.; Mauriello, C.; Pascucci, E.; Savino, M.; Ortaggi, G.; Bianco, A. Specific interactions with intra- and intermolecular G-quadruplex DNA structures by hydrosoluble coronene derivatives: a new class of telomerase inhibitors. *Bioorg. Med. Chem.* **2007**, *15*, 1848–1858.
(95) Ladame, S.; Schouten, J. A.; Stuart, J.; Roldan, J.; Neidle, S.; Balasubramanian, S. Tetrapeptides induce selective recognition for G-quadruplexes when conjugated to a DNA-binding platform. *Org. Biomol. Chem.* **2004**, *2*, 2925–2931.
(96) *Affinity*; Molecular Simulations Inc.: San Diego, CA, 2000.
(97) Watson, J. D.; Crick, F. H. Molecular structure of nucleic acids; a structure for deoxyribose nucleic acid. *Nature* **1953**, *171*, 737–738.
(98) Reed, J. E.; Gunaratnam, M.; Beltran, M.; Reszka, A. P.; Vilar, R.; Neidle, S. TRAP-LIG, a modified TRAP assay to quantitate telomerase inhibition by small molecules. *Anal. Biochem.*, published online 2008, http://dx.doi.org/10.1016//j.ab.2008.05.013.
(99) Papazisis, K. T.; Geromichalos, G. D.; Dimitriadis, K. A.; Kortsaris, A. H. Optimization of the sulforhodamine B colorimetric assay. *J. Immunol. Methods* **1997**, *208*, 151–158.
(100) Skehan, P.; Storeng, R.; Scudiero, D.; Monks, A.; McMahon, J.; Vistica, D.; Warren, J. T.; Bokesch, H.; Kenney, S.; Boyd, M. R. New colorimetric cytotoxicity assay for anticancer-drug screening. *J. Natl. Cancer Inst.* **1990**, *82*, 1107–1112.
(101) Dimri, G. P.; Lee, X.; Basile, G.; Acosta, M.; Scott, G.; Roskelley, C.; Medrano, E. E.; Linskens, M.; Rubelj, I.; Pereira-Smith, O.; Peacocke, M.; Campisi, J. A biomarker that identifies senescent human cells in culture and in aging skin in vivo. *Proc. Natl. Acad. Sci. U.S.A.* **1995**, *92*, 9363–9367.
(102) Choo, H. Y.; Kim, M.; Lee, S. K.; Kim, S. W.; Chung, I. K. Solid-phase combinatorial synthesis and cytotoxicity of 3-aryl-2,4-quinazolindiones. *Bioorg. Med. Chem.* **2002**, *10*, 517–523.
(103) Jo, M. N.; Seo, H. J.; Kim, Y.; Seo, S. H.; Rhim, H.; Cho, Y. S.; Cha, J. H.; Koh, H. Y.; Choo, H.; Pae, A. N. Novel T-type calcium channel blockers: dioxoquinazoline carboxamide derivatives. *Bioorg. Med. Chem.* **2007**, *15*, 365–373.
(104) Kakuta, H.; Tanatani, A.; Nagasawa, K.; Hashimoto, Y. Specific nonpeptide inhibitors of puromycin-sensitive aminopeptidase with a 2,4(1*H*,3*H*)-quinazolinedione skeleton. *Chem. Pharm. Bull.* **2003**, *51*, 1273–1282.
(105) Peet, N. P.; Sunder, S. Phosgenation of methyl anthranilate. *J. Org. Chem.* **1974**, *39*, 1931–1935.
(106) Rachwal, P. A.; Fox, K. R. Quadruplex melting. *Methods* **2007**, *43*, 291–301.
(107) Neidle, S. DNA minor-groove recognition by small molecules. *Nat. Prod. Rep.* **2001**, *18*, 291–309.
(108) Dai, Y.; Hartandi, K.; Ji, Z.; Ahmed, A. A.; Albert, D. H.; Bauch, J. L.; Bouska, J. J.; Bousquet, P. F.; Cunha, G. A.; Glaser, K. B.; Harris, C. M.; Hickman, D.; Guo, J.; Li, J.; Marcotte, P. A.; Marsh, K. C.; Moskey, M. D.; Martin, R. L.; Olson, A. M.; Osterling, D. J.; Pease, L. J.; Soni, N. B.; Stewart, K. D.; Stoll, V. S.; Tapang, P.; Reuter, D. R.; Davidsen, S. K.; Michaelides, M. R. Discovery of *N*-(4-(3-amino-1*H*-indazol-4-yl)phenyl)-*N*′-(2-fluoro-5-methylphenyl)urea (ABT-869), a 3-aminoindazole-based orally active multitargeted receptor tyrosine kinase inhibitor. *J. Med. Chem.* **2007**, *50*, 1584–1597.
(109) Gable, K. L.; Maddux, B. A.; Penaranda, C.; Zavodovskaya, M.; Campbell, M. J.; Lobo, M.; Robinson, L.; Schow, S.; Kerner, J. A.; Goldfine, I. D.; Youngren, J. F. Diarylureas are small-molecule inhibitors of insulin-like growth factor I receptor signaling and breast cancer cell growth. *Mol. Cancer Ther.* **2006**, *5*, 1079–1086.
(110) Ambrus, A.; Chen, D.; Dai, J.; Bialis, T.; Jones, R. A.; Yang, D. Human telomeric sequence forms a hybrid-type intramolecular G-quadruplex structure with mixed parallel/antiparallel strands in potassium solution. *Nucleic Acids Res.* **2006**, *34*, 2723–2735.
(111) Phan, A. T.; Kuryavyi, V.; Luu, K. N.; Patel, D. J. Structure of two intramolecular G-quadruplexes formed by natural human telomere sequences in K^+ solution. *Nucleic Acids Res.* **2006**, *35*, 6517–6525.
(112) Dai, J.; Carver, M.; Punchihewa, C.; Jones, R. A.; Yang, D. Structure of the hybrid-2 type intramolecular human telomeric G-quadruplex in K^+ solution: insights into structure polymorphism of the human telomeric sequence. *Nucleic Acids Res.* **2007**, *35*, 4927–4740.
(113) Drewe, W. C.; Neidle, S. Click chemistry assembly of G-quadruplex ligands incorporating a diarylurea scaffold and triazole linkers. *Chem. Commun.*, 5295−5297.
(114) Xue, Y.; Kan, Z. Y.; Wang, O.; Yao, Y.; Liu, J.; Hao, Y. H.; Tan, Z. Human telomeric DNA forms parallel-stranded intramolecular G-quadruplex in K+ solution under molecular crowding condition. *J. Am. Chem. Soc.* **2007**, *129*, 11185–11191.
(115) Parkinson, G. N.; Cuenca, F.; Neidle, S. Topology conservation and loop flexibility in quadruplex−drug recognition: crystal structures of inter- and intramolecular telomeric DNA quadruplex−drug complexes. *J. Mol. Biol.* **2008**, *381*, 1145–1156.

JM801245V